

POLITECNICO DI TORINO

Collegio di Ingegneria Energetica

**Corso di Laurea Magistrale
in Ingegneria Energetica e Nucleare**



Tesi di Laurea Magistrale

Development of directly assembled composite oxygen electrodes for reversible solid oxide fuel cells

Relatore
prof. Massimo Santarelli

Candidato
Giulio Maurizio

Corelatore
prof. San Ping Jiang

Luglio 2018

Alla mia famiglia

Contents

I	List of Figures.....	III
II	List of Tables.....	VII
III	Abstract.....	IX
1	Introduction	1
2	Electrochemical model	3
2.1	Electrochemical cell.....	3
2.2	Open circuit potential.....	3
2.2.1	Gibbs free energy	3
2.2.2	Nernst equation.....	6
2.3	Efficiency.....	7
2.4	Polarization losses.....	9
2.4.1	Activation losses.....	10
2.4.2	Ohmic losses.....	11
2.4.3	Mass transport or concentration losses.....	12
2.4.4	Fuel crossover and internal currents.....	13
2.4.5	Combining the irreversibilities	13
3	Fuel cell technologies	15
3.1	Low temperature fuel cells	15
3.1.1	Alkaline fuel cells.....	15
3.1.2	Proton exchange membrane fuel cells.....	16
3.1.3	Phosphoric acid fuel cells	16
3.2	Medium and high temperature fuel cells	16
3.2.1	Molten carbonate fuel cells	16
3.2.2	Solid oxide fuel cells	17
4	Solid oxide fuel cells	19
4.1	Electrolyte.....	20
4.2	Anode.....	20
4.3	Cathode	21
4.3.1	LSM.....	21
4.3.2	LSCF.....	22
4.3.3	BSCF	22
4.3.4	NBCaC	22
4.3.5	Composite cathodes.....	23
5	Experimental.....	25
5.1	Samples fabrication.....	25

5.1.1	In-situ vs pre-sintered approach.....	27
5.2	Experimental tests	28
5.2.1	Electrochemical impedance spectroscopy	29
5.2.2	Galvanostatic polarization	32
5.2.3	Open circuit potential.....	32
5.2.4	Interface analysis	32
6	Results.....	33
6.1	LSM.....	33
6.1.1	LSM/YSZ.....	33
6.1.2	LSM/GDC.....	36
6.2	LSCF	39
6.2.1	LSCF/YSZ	39
6.2.2	LSCF/GDC	40
6.3	BSCF	43
6.3.1	BSCF/YSZ	44
6.3.2	BSCF/GDC	47
6.4	NBCaC	50
6.4.1	NBCaC/YSZ	51
6.4.2	NBCaC/GDC	54
7	Conclusions.....	59
8	Bibliography	61
9	Ringraziamenti.....	65

I List of Figures

Figure 1 - Simple schematic of a Galvanic (a) cell and an electrolytic cell (b)	3
Figure 2 - Comparison between fuel cell efficiency limit and Carnot limit	8
Figure 3 - Typical polarization curve of a fuel cell	9
Figure 4 - Typical polarization curve of an electrolytic cell	14
Figure 5 - Fuel cell types, showing the general trend of their features	15
Figure 6 - Operation diagram of a SOFC	19
Figure 7 - Comparison of the three-phase boundary regions of different SOFC anode materials	21
Figure 8 - Crystal structure of LSM	21
Figure 9 - Crystal structure of NBCaC	22
Figure 10 - Three-electrodes half-cell setup	25
Figure 11 - YSZ electrolyte disc die pressing	25
Figure 12 - YSZ electrolyte discs before (left) and after (right) sintering procedure	26
Figure 13 - Reference and counter electrode	26
Figure 14 - Working electrode application on YSZ electrolyte disc by slurry coating	27
Figure 15 - Pre-sintered vs in-situ approach	28
Figure 16 - Three electrodes setup	29
Figure 17 - Simplified Randles cell circuit and relative Nyquist plot	31
Figure 18 - Impedance and polarization curves of LSM pristine electrode, on YSZ electrolyte under 250 mAcm^{-2} of cathodic current density	33
Figure 19 - Impedance and polarization curves of LSM/YSZ composite electrode, on YSZ electrolyte under 250 mAcm^{-2} of cathodic current density	33
Figure 20 - Impedance and polarization curves of LSM/YSZ composite electrode, on YSZ electrolyte under 500 mAcm^{-2} of cathodic current density	34
Figure 21 - SEM images of YSZ electrolyte surface after 12 hours of cathodic polarization. Red circles highlight LSM particles	34
Figure 22 - Impedance and polarization curves of LSM/YSZ composite electrode, on YSZ electrolyte under 250 mAcm^{-2} of anodic current density	34
Figure 23 - Impedance and polarization curves of LSM/YSZ composite electrode, on YSZ electrolyte under 500 mAcm^{-2} of anodic current density	35
Figure 24 - SEM images of YSZ electrolyte surface after 12 hours of cathodic polarization. Red circles highlight the strain stresses accumulated during the YSZ pressing procedure	35
Figure 25 - Impedance and polarization curves of LSM/YSZ composite electrode, on YSZ electrolyte before and after 12 hours of open circuit potential	35
Figure 26 - SEM images of YSZ electrolyte surface after 12 hours of open circuit potential	36
Figure 27 - Impedance and polarization curves of LSM/GDC composite electrode, on YSZ electrolyte under	36
Figure 28 - Impedance and polarization curves of LSM/GDC composite electrode, on YSZ electrolyte under	37
Figure 29 - SEM images of YSZ electrolyte surface after 12 hours of cathodic polarization	37
Figure 30 - Impedance and polarization curves of LSM/GDC composite electrode, on YSZ electrolyte under	37
Figure 31 - Impedance and polarization curves of LSM/GDC composite electrode, on YSZ electrolyte under	38

Figure 32 - SEM images of YSZ electrolyte surface after 12 hours of anodic polarization. Red circles highlight the presence of little holes on the YSZ surface	38
Figure 33 - Impedance and polarization curves of LSM/GDC composite electrode, on YSZ electrolyte before and after 12 hours of open circuit potential	38
Figure 34 - SEM images of YSZ electrolyte surface after 12 hours of open circuit potential	39
Figure 35 - Impedance and polarization curves of LSCF pristine electrode, on YSZ electrolyte under 250 mAcm ⁻² of cathodic current density	39
Figure 36 - Impedance and polarization curves of LSCF/YSZ composite electrode, on YSZ electrolyte under	40
Figure 37 - Impedance and polarization curves of LSCF/YSZ composite electrode, on YSZ electrolyte under	40
Figure 38 - Impedance and polarization curves of LSCF/YSZ composite electrode, on YSZ electrolyte before and after 12 hours of open circuit potential	40
Figure 39 - Impedance and polarization curves of LSCF/GDC composite electrode, on YSZ electrolyte under 250 mAcm ⁻² of cathodic current density	41
Figure 40 - Impedance and polarization curves of LSCF/GDC composite electrode, on YSZ electrolyte under 500 mAcm ⁻² of cathodic current density	41
Figure 41 - SEM images of YSZ electrolyte surface after 12 hours of cathodic polarization	41
Figure 42 - Impedance and polarization curves of LSCF/GDC composite electrode, on YSZ electrolyte under 250 mAcm ⁻² of anodic current density	42
Figure 43 - Impedance and polarization curves of LSCF/GDC composite electrode, on YSZ electrolyte under 500 mAcm ⁻² of anodic current density	42
Figure 44 - SEM images of YSZ electrolyte surface after 12 hours of anodic polarization	42
Figure 45 - Impedance and polarization curves of LSCF/GDC composite electrode, on YSZ electrolyte before and after 12 hours of open circuit potential	43
Figure 46 - SEM images of YSZ electrolyte surface after 12 hours of open circuit potential	43
Figure 47 - Impedance and polarization curves of BSCF pristine electrode, on YSZ electrolyte under 250 mAcm ⁻² of cathodic current density	43
Figure 48 - XRD thermochemical compatibility test between BSCF and YSZ	44
Figure 49 - Impedance and polarization curves of BSCF/YSZ composite electrode, on YSZ electrolyte under	44
Figure 50 - Impedance and polarization curves of BSCF/YSZ composite electrode, on YSZ electrolyte under	45
Figure 51 - SEM images of YSZ electrolyte surface after 12 hours of cathodic polarization	45
Figure 52 - Impedance and polarization curves of BSCF/YSZ composite electrode, on YSZ electrolyte under	45
Figure 53 - Impedance and polarization curves of BSCF/YSZ composite electrode, on YSZ electrolyte under	46
Figure 54 - SEM images of YSZ electrolyte surface after 12 hours of anodic polarization	46
Figure 55 - Impedance and polarization curves of BSCF/YSZ composite electrode, on YSZ electrolyte before and after 12 hours of open circuit potential	46
Figure 56 - SEM images of YSZ electrolyte surface after 12 hours of open circuit potential	47
Figure 57 - XRD thermochemical compatibility test between BSCF and GDC	47

Figure 58 - Impedance and polarization curves of BSCF/GDC composite electrode, on YSZ electrolyte under 250 mAcm ⁻² of cathodic current density	48
Figure 59 - Impedance and polarization curves of BSCF/GDC composite electrode, on YSZ electrolyte under 500 mAcm ⁻² of cathodic current density	48
Figure 60 - SEM images of YSZ electrolyte surface after 12 hours of cathodic polarization	48
Figure 61 - Impedance and polarization curves of BSCF/GDC composite electrode, on YSZ electrolyte under 250 mAcm ⁻² of anodic current density	49
Figure 62 - Impedance and polarization curves of BSCF/GDC composite electrode, on YSZ electrolyte under 500 mAcm ⁻² of anodic current density	49
Figure 63 - SEM images of YSZ electrolyte surface after 12 hours of anodic polarization	49
Figure 64 - Impedance and polarization curves of BSCF/GDC composite electrode, on YSZ electrolyte before and after 12 hours of open circuit potential	50
Figure 65 - SEM images of YSZ electrolyte surface after 12 hours of open circuit potential	50
Figure 66 - Impedance and polarization curves of NBCaC pristine electrode, on YSZ electrolyte under 250 mAcm ⁻² of cathodic current density	50
Figure 67 - XRD thermochemical compatibility test between NBCaC and YSZ	51
Figure 68 - Impedance and polarization curves of NBCaC/YSZ composite electrode, on YSZ electrolyte under 250 mAcm ⁻² of cathodic current density	51
Figure 69 - Impedance and polarization curves of NBCaC/YSZ composite electrode, on YSZ electrolyte under 500 mAcm ⁻² of cathodic current density	51
Figure 70 - SEM images of YSZ electrolyte surface after 12 hours of cathodic polarization	52
Figure 71 - Impedance and polarization curves of NBCaC/YSZ composite electrode, on YSZ electrolyte under 250 mAcm ⁻² of anodic current density	52
Figure 72 - Impedance and polarization curves of NBCaC/YSZ composite electrode, on YSZ electrolyte under 500 mAcm ⁻² of anodic current density	52
Figure 73 - SEM images of YSZ electrolyte surface after 12 hours of anodic polarization	53
Figure 74 - Impedance and polarization curves of NBCaC/YSZ composite electrode, on YSZ electrolyte before and after 12 hours of open circuit potential	53
Figure 75 - SEM images of YSZ electrolyte surface after 12 hours of open circuit potential	53
Figure 76 - Impedance and polarization curves of NBCaC/GDC composite electrode, on YSZ electrolyte under 250 mAcm ⁻² of cathodic current density	54
Figure 77 - Impedance and polarization curves of NBCaC/GDC composite electrode, on YSZ electrolyte under 500 mAcm ⁻² of cathodic current density	54
Figure 78 - SEM images of YSZ electrolyte surface after 12 hours of cathodic polarization	55
Figure 79 - Impedance and polarization curves of NBCaC/GDC composite electrode, on YSZ electrolyte under 250 mAcm ⁻² of anodic current density	55
Figure 80 - Impedance and polarization curves of NBCaC/GDC composite electrode, on YSZ electrolyte under 500 mAcm ⁻² of anodic current density	55
Figure 81 - SEM images of YSZ electrolyte surface after 12 hours of anodic polarization	56
Figure 82 - Impedance and polarization curves of NBCaC/GDC composite electrode, on YSZ electrolyte before and after 12 hours of open circuit potential	56

Figure 83 - SEM images of YSZ electrolyte surface after 12 hours of open circuit potential

56

II List of Tables

Table 1 - Gibbs free energy of formation at standard conditions	5
Table 2 - Efficiency limits for hydrogen fuel cell	8
Table 3 - Electrochemical and mechanical properties of the investigated materials	23
Table 4 - Impedance of circuit elements	30

III Abstract

Le celle ad ossidi solidi (SOC) rappresentano una tra le più efficienti tecnologie di conversione dell'energia chimica direttamente in energia elettrica, e viceversa. Infatti, possono operare sia come fuel cell (SOFC) sia come elettrolizzatori (SOEC). La reversibilità è un aspetto molto interessante di questi dispositivi.

Come ogni altra cella elettrochimica, le SOC sono composte da due elettrodi separati da un elettrolita, in generale zirconia stabilizzata con ossidi di ittrio (YSZ), che, nel range di temperature comprese tra 600 °C e 1000 °C, funziona da conduttore di ioni. L'elettrodo a contatto con il combustibile è solitamente composto da ossidi di nichel mescolati a YSZ. Il YSZ aiuta a bloccare la crescita dei grani del nichel, che altrimenti andrebbero a ridurre l'area di contatto attraverso la quale gli ioni possono essere trasportati. L'anodo (o catodo in modalità elettrolisi) è solitamente lo strato più forte e spesso in ogni singola cella, perché è proprio lo strato che comporta le minor perdite di polarizzazione. Il materiale più comune utilizzato nella fabbricazione dei catodi delle fuel cell ad ossidi solidi è la manganite di lantanio e stronzio (LSM), per la sua buona conduttività elettronica ad alte temperature.¹ Tuttavia, le sue prestazioni diminuiscono rapidamente se la temperatura operativa scende sotto gli 800 °C. Infatti, ridurre la temperatura operativa significa risparmiare più energia, e perciò è diventata la nuova sfida nello sviluppo delle SOC. La selezione di un materiale adatto ad essere utilizzato come catodo nelle SOFC a medio-bassa temperatura può anche espandere il three-phase boundary (TPB). Nel caso del LSM, infatti, a causa della sua trascurabile conduttività ionica, il TPB è limitato alla sola interfaccia tra catodo ed elettrolita.

Perciò, è di fondamentale importanza lo studio dei materiali in grado di offrire un'elevata conduttività elettronica a basse temperature. I cosiddetti MIEC (mixed ionic electronic conductors) sono ottimi candidati per questo scopo. I MIEC possono aiutare a sviluppare TPB più ampi e di conseguenza SOFC a medio-bassa temperatura più performanti.²

La concentrazione della maggior parte delle perdite di polarizzazione nel catodo e le nuove possibilità offerte dagli elettrodi compositi sono le ragioni principali per cui questo studio è focalizzato sullo studio di mezze celle soltanto. In questo studio, diversi materiali sono stati studiati: manganite di lantanio e stronzio, cobaltite-ferrite di lantanio e stronzio (LSCF), cobaltite-ferrite di bario e stronzio (BSCF) cobaltite-calcite di neodimio e bario (NBCaC), mischiati una volta con YSZ e una volta con ceria drogata con ossidi di gadolinio (GDC).

A differenza dei più comuni metodi utilizzati per la fabbricazione delle SOFC, in questo studio, gli elettrodi soggetti di studio sono stati direttamente applicati sull'elettrolita per mezzo di una procedura in-situ, che non prevede processi di sinterizzazione. In questo modo, è possibile evitare diversi step, risparmiando energia, tempo e denaro, e soprattutto non c'è pericolo di dar vita a nuove fasi generate da reazioni chimiche tra elettrodo ed elettrolita dovute all'alta temperatura dei processi di sinterizzazione. Nonostante questi vantaggi, senza un processo di sinterizzazione ad alta temperatura non è possibile creare un contatto intimo tra elettrodo ed elettrolita.³ Perciò, l'interfaccia è stata creata attraverso il passaggio di corrente catodica (modalità

fuel cell) o anodica (modalità anodica). Altre analisi, come la spettroscopia dell'impedenza elettrochimica (EIS) e la microscopia elettronica a scansione (SEM), sono state portate avanti per studiare le prestazioni delle celle e l'evoluzione dell'interfaccia elettrodo/elettrolita.

1 Introduction

Solid oxide cells (SOCs) are one of the most efficient technologies for the conversion of chemical energy directly into electrical energy, and vice versa. Indeed, they can operate both as fuel cells (SOFCs) and as electrolyzers (SOECs). The reversibility is a very interesting aspect of these devices.

Like any other electrochemical cell, SOCs are composed of two electrodes separated by an electrolyte, usually yttria-stabilized zirconia (YSZ), that serves as an ionic conductor in the temperature range between 600 °C to 1000 °C. The fuel electrode is usually made of nickel oxide mixed with YSZ. YSZ helps stop the grain growth of nickel that would reduce the contact area that ions can be conducted through. Fuel electrode is commonly the thickest and strongest layer in each individual cell, because it has the smallest polarization losses. The most common material used in the fabrication of oxygen electrode is lanthanum strontium manganite (LSM), because of its high electronic conductivity at high temperatures.¹ However, its performances degrade quickly as the operating temperature goes down 800 °C. Indeed, reducing the operating temperature means saving more energy, and therefore has become the new aim in SOCs development. Moreover, a lower temperature requires cheaper materials. The selection of a suitable cathode material for an intermediate to low temperature SOC (IT-LTSOC) can also enlarge the three-phase boundary (TPB) that in the case of LSM oxygen electrode, since its negligible oxygen ion conductivity, is limited at the interface between the electrode and the electrolyte.

Therefore, it is fundamental studying oxygen electrode component materials offering higher electron conductivity at lower operating temperatures. Mixed ionic-electronic conductors (MIECs) are good candidates for this purpose. MIECs may help develop larger TPBs and increase the performance of IT-LTSOCs.²

The concentration of most of the polarization losses in the oxygen electrode and the new possibilities offered by composite electrodes are the main reasons why this work is mainly focused on the study of half-cells only (electrolyte and oxygen electrode only). In this study, different oxygen electrode materials are investigated: lanthanum strontium manganite, lanthanum strontium cobalt ferrite (LSCF), barium strontium cobalt ferrite (BSCF) and neodymium barium calcium cobaltite (NBCaC), mixed with some common oxygen ions conductors, once with yttria-stabilized zirconia and once with gadolinium-doped ceria.

Unlike the most common ways to fabricate the oxygen electrode, in this study the oxygen electrode was directly applied on the electrolyte through an in situ procedure, without sintering it. In this way several steps are skipped, saving energy, time and money, and moreover there is no danger of producing new phases between the electrode and the electrolyte due to the high temperatures of the sintering process. Despite of these advantages, without a sintering process at high temperature is not possible to create an intimate electrode/electrolyte contact.³ Thus, the interface was created with the passage of cathodic (fuel cell mode) or anodic (electrolysis mode) current. Further analysis, such as electrochemical impedance spectroscopy (EIS) and scanning electron microscopy (SEM)

were carried on in order to study the cells performance and the evolution of the electrolyte/oxygen electrode interface.

2 Electrochemical model

2.1 Electrochemical cell

An electrochemical cell is a device capable of either generating electrical energy from chemical reactions (Galvanic cell) or facilitating non-spontaneous chemical reactions through the introduction of electrical energy (electrolytic cell). Each electrochemical cell is composed by two half-cells. Every half-cell consists of an electrode and an electrolyte. In the case of SOCs, the two half-cells share the same electrolyte. In a full electrochemical cell, species from one half-cell lose electrons (oxidation) to their electrode while species from the other half-cell gain electrons (reduction) from their electrode. Fuel cells and electrolyzers, since reactants come from outside and products leave immediately the cell, are examples of open electrochemical cells.

Each half-cell has a characteristic voltage. Each reaction is undergoing an equilibrium reaction between different oxidation states of the ions: when equilibrium is reached, the cell cannot provide further voltage. In the half-cell that is undergoing oxidation, the closer the equilibrium lies to the ion/atom with the more positive oxidation state the more potential this reaction will provide. Likewise, in the reduction reaction, the closer the equilibrium lies to the ion/atom with the more negative oxidation state, the higher the potential. Figure 1 shows a very simple representation of the two type of electrochemical cells, Galvanic and electrolytic.⁴

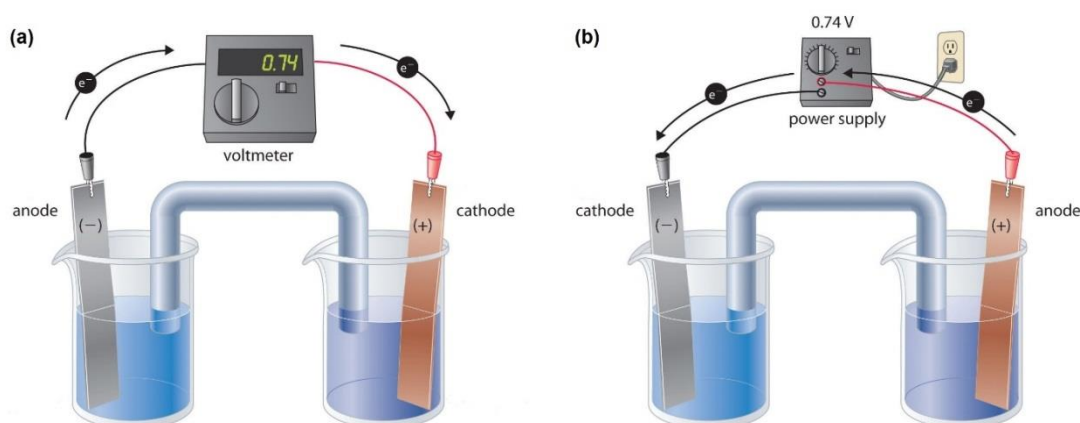


Figure 1 - Simple schematic of a Galvanic (a) cell and an electrolytic cell (b)

2.2 Open circuit potential

The open circuit potential (OCP) of an electrochemical cell is the difference of electrical potential between the two electrodes disconnected from any circuit, so that no external load is connected. In order to calculate it, it is fundamental to introduce two important concepts: the Gibbs free energy and the Nernst equation.

2.2.1 Gibbs free energy

Gibbs free energy is a state function used in thermodynamics to express the free energy in isothermobaric transformations (constant temperature and constant pressure, as well as the most chemical reactions), and it determines the spontaneity of a reaction. This state function allows to establish the useful work obtainable from a transformation of a thermodynamic system at constant temperature and constant pressure. The equivalent function in mechanic is the potential energy. In a similar way, the Gibbs free energy is the

maximum quantity of work, not due to the mechanical expansion, available from a closed system. The maximum work is achievable exclusively if the transformations are reversible. A thermodynamic system at constant temperature and constant pressure reaches the thermodynamic equilibrium when the Gibbs free energy reaches its minimum.

The Gibbs free energy is defined as

$$G(p, T) = U + pV - TS \quad (1)$$

and since

$$H = U + pV \quad (2)$$

the Gibbs free energy is also expressed as

$$G(p, T) = H - TS \quad (3)$$

where:

- U is the internal energy [J];
- p is pressure [Pa];
- V is volume [m³];
- T is the temperature [K];
- S is the entropy [J/K];
- H is the enthalpy [J].

The total differential becomes

$$dG = dU + pdV + Vdp - TdS - SdT \quad (4)$$

Considering the first law of thermodynamics

$$dU = \delta Q + \delta W \quad (5)$$

where δQ is energy added as heat and δW is energy added as work, and assuming only mechanical work is done

$$\delta W = -pdV \quad (6)$$

and considering no changes in pressure and temperature, the Gibbs free energy differential becomes

$$dG = \delta Q - TdS \quad (7)$$

The second law of thermodynamics states that for a closed system

$$TdS \geq \delta Q \quad (8)$$

and so, it follows

$$dG \leq 0 \quad (9)$$

This means that for a system which is not in equilibrium, its Gibbs free energy will be decreasing until it reaches the equilibrium.

For an ideal gas that changes its state in a reversible ($\delta Q, dS = 0$) way at constant temperature, from equations 4, 5 and 6

$$dG = Vdp \quad (10)$$

From ideal gas law

$$pV = RT \quad (11)$$

equation 10 becomes

$$dG = \frac{RT}{p} dp \quad (12)$$

and integrating between p_0 and p_{final}

$$\Delta G = G_2 - G_1 = RT \ln \left(\frac{p}{p_0} \right) \quad (13)$$

thus

$$G = G^0 + RT \ln(p) \quad (14)$$

In the case of a real gas, pressure is replaced by activity

$$G = G^0 + RT \ln(a) \quad (15)$$

For the formation reaction of water, involved into the fuel cell systems, the molar Gibbs free energy ($\Delta \bar{g}_f$) can be expressed as

$$\Delta \bar{g}_f = \bar{g}_{H_2O} - \bar{g}_{H_2} - 0.5 \bar{g}_{O_2} \quad (16)$$

Where the coefficients of equation 16 come directly from water formation reaction



Table 1 reports the Gibbs free energy of formation at standard conditions.

Chemical species	Gibbs free energy [kJ mol ⁻¹]
H ₂	0
O ₂	0
H ₂ O	-237.18

Table 1 - Gibbs free energy of formation at standard conditions

Since hydrogen and oxygen are pure elements, their Gibbs free energy of formation is zero.⁵ Consequently

$$\Delta \bar{g}_f = \bar{g}_{H_2O} = -237.18 \frac{kJ}{mol} \quad (18)$$

2.2.2 Nernst equation

In electrochemistry, Nernst equation is very useful for calculating the electrode potential in nonstandard conditions. Its general form is the following

$$E = E^0 + \frac{RT}{ZF} \ln \left[\frac{\prod (a_{i,ox}^{v_{ox}})}{\prod (a_{i,red}^{v_{red}})} \right] \quad (19)$$

where:

- R is the universal gas constant [8.314 J/(Kmol)];
- T is the temperature [K];
- $a_{i,red}$ is the chemical activity of the i-th species in its reduced form;
- $a_{i,ox}$ is the chemical activity of the i-th species in its oxidized form;
- v_{red} and v_{ox} are their stoichiometric coefficients;
- Z is the number of the electrons involved in the semi reaction;
- F is the Faraday constant [96485 C/mol];
- E^0 is the standard electrode potential of the considered chemical species.

Nernst equation is based on thermodynamics bases. Let's consider a reduction reaction that involves a generic metal Me



where an oxidized species Me^{n+} acquires Z electrons producing the reduced species Me. A Gibbs free energy variation corresponds to this reaction, and it is equal to

$$\Delta G = \Delta G^0 + RT \ln \frac{a_{Me}}{a_{Me^{n+}}} \quad (21)$$

The Gibbs free energy is linked to the useful work. In the case of electrical work, the relation between the two is

$$\Delta G = -ZF\Delta E \quad (22)$$

Every standard electrode potentials are always referred to the hydrogen standard electrode, that for definition

$$E^0 = 0V \quad (23)$$

Therefore

$$\Delta E = E \quad (24)$$

and

$$\Delta E^0 = E^0 \quad (25)$$

From equations 21, 22 and 24

$$\Delta G^0 + RT \ln \frac{a_{Me}}{a_{Me^{n+}}} = -ZFE \quad (26)$$

Isolating the reduction potential

$$E = -\frac{\Delta G^0}{ZF} - \frac{RT}{ZF} \ln \frac{a_{Me}}{a_{Me^{n+}}} \quad (27)$$

The first term is constant, and it represents the standard reduction potential E^0 . Replacing and generalizing, equation 16 is obtained.⁶

In the case of a hydrogen fuel cell, the OCP at standard conditions is calculated applying the reduced form of Nernst equation

$$E = -\frac{\Delta \bar{g}_f}{ZF} = \frac{-\left(237.18 \frac{kJ}{mol}\right)}{2 * 96485 \frac{C}{mol}} = 1.23V \quad (28)$$

2.3 Efficiency

Summing up, it is the Gibbs free energy that is converted into electrical energy (fuel cell) or vice versa (electrolyser). It has been shown that Gibbs free energy changes mainly with temperature and pressure. Thus, it is not very useful to define the efficiency of a fuel cell as the ratio between the electrical energy produced and the Gibbs free energy change. Since a fuel cell uses materials that are usually burnt to release their energy, it would make sense to compare the electrical energy produced with the heat that would be produced by burning the fuel, the so-called change in enthalpy of formation ($\Delta \bar{h}_f$, molar quantity). As with the Gibbs free energy, the convention is that $\Delta \bar{h}_f$ is negative when energy is released. So, to get a good comparison with other fuel-using technologies, the efficiency of the fuel cell is usually defined as

$$\eta = \frac{\text{electrical energy produced per mole of fuel}}{-\Delta \bar{h}_f} \quad (29)$$

Typically, two different values of $\Delta \bar{h}_f$ are given, respectively if they are referred to the lower heating value (LHV) or to the higher heating value (HHV). Usually, the use of LHV is preferred, since this will give a higher efficiency.

Looking at equation 29, is possible to notice that there is a limit for the efficiency. Indeed, the maximum electrical energy achievable is exactly the variation of the Gibbs free. So that

$$\eta_{max} = \frac{\Delta \bar{g}_f}{\Delta \bar{h}_f} \quad (30)$$

Table 2 gives the values of the efficiency limit, relative to the HHV, for a hydrogen fuel cell. The relative maximum voltage is also given.

Water product	Temperature [°C]	$\Delta \bar{h}_f$ [kJ mol ⁻¹]	OCP _{max} [V]	Efficiency limit [%]
Liquid	25	-237.2	1.23	83
Liquid	80	-228.2	1.18	80
Gas	100	-225.2	1.17	79
Gas	200	-220.4	1.14	77
Gas	400	-210.3	1.09	74
Gas	600	-199.6	1.04	70
Gas	800	-188.6	0.98	66
Gas	1000	-177.4	0.92	62

Table 2 - Efficiency limits for hydrogen fuel cell

The graph in Figure 2 shows how the efficiency values vary with temperature, and how they compare with the ‘Carnot limit’.

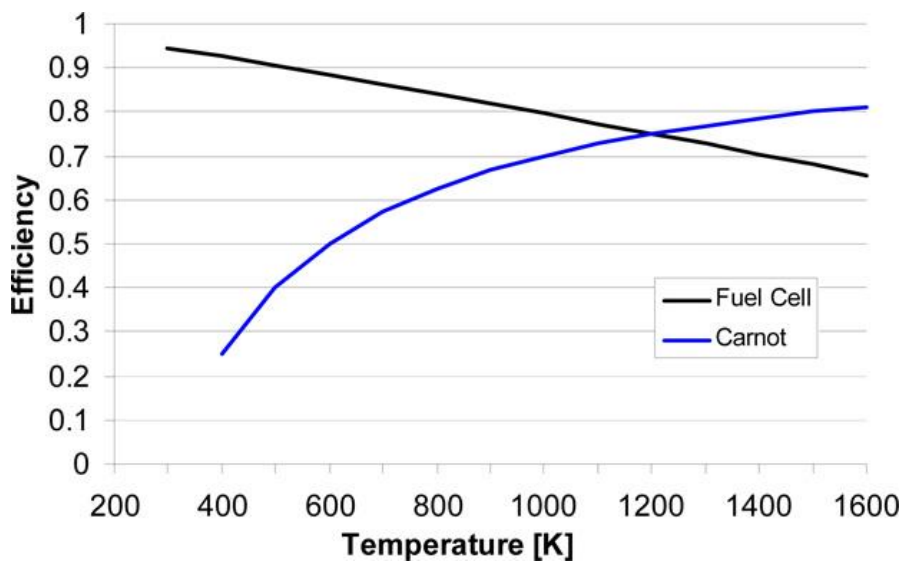


Figure 2 - Comparison between fuel cell efficiency limit and Carnot limit

Two important points should be noted:

- although Table 2 and Figure 2 would suggest that lower temperatures are better, the voltage losses discussed in next pages are nearly always less at higher temperatures. So in practice fuel cell voltages are usually higher at higher temperatures;
- the waste heat from the higher-temperature cells is always more useful than that coming from lower-temperature cells.

It is clear from Table 2 that there is a connection between the maximum OCP of a cell and its maximum efficiency. The operating voltage of a fuel cell can also be very easily related to its efficiency. With reference to LHV

$$\eta = \frac{V_c}{1.23V} \quad (31)$$

However, in practice it is found that not all the fuel that is fed to a fuel cell can be used. Some fuel usually has to pass through unreacted. A fuel utilisation coefficient can be defined as

$$\mu_f = \frac{\text{mass of fuel reacted in cell}}{\text{mass of fuel fed to cell}} \quad (32)$$

Equation 31 is therefore modified in

$$\eta = \mu_f \frac{V_c}{1.23V} \quad (33)$$

A good estimation for μ_f is 0.95, which allows the efficiency of a fuel cell to be accurately estimated from the very simple measurement of its voltage.⁷

2.4 Polarization losses

Although a fuel cell at open circuit has an incredible voltage, when it is connected to an external load and current starts flowing, it is found that the voltage drops in accordance to the current. As shown in Figure 3, there are different phenomena that cause a voltage drop.

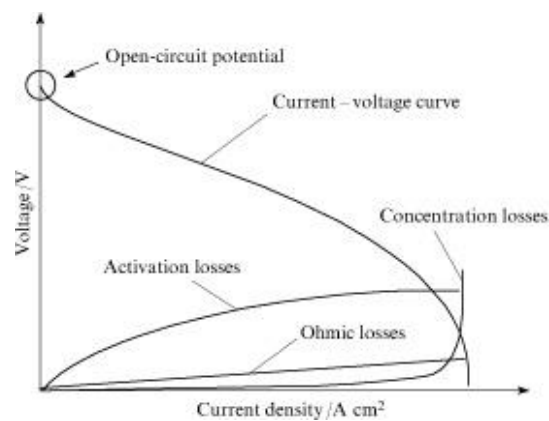


Figure 3 - Typical polarization curve of a fuel cell

The key points to notice about the graph of the cell voltage against current density are as follows:

- even the open circuit potential is less than the theoretical value;
- there is a rapid initial fall in voltage;
- the voltage then falls less rapidly and more linearly;
- there is sometimes a higher current density at which the voltage falls rapidly.

The characteristic shape of the voltage/current density graph results from four major irreversibilities:

- Activation losses. These are caused by the slowness of the reactions taking place on the surface of the electrodes. A proportion of the voltage generated is lost in driving the chemical reaction that transfers the electrons to or from the electrode. This voltage drop is highly non-linear.
- Ohmic losses. This voltage drop is the straightforward resistance to the flow of electrons through the material of the electrodes and the various interconnections, as well as the resistance to the flow of ions through the electrolyte. This voltage drop is essentially proportional to current density, linear, and so is called ohmic losses, or sometimes as resistive losses.

- Mass transport or concentration losses. These result from the change in concentration of the reactants at the surface of the electrodes as the fuel is used. As stated by Nernst equation, concentration affects voltage, and so this type of irreversibility is sometimes called concentration loss. Because the reduction in concentration is the result of a failure to transport sufficient reactant to the electrode surface, this type of loss is also often called mass transport loss. This type of loss has a third name – ‘Nernstian’. This is because of its connections with concentration, and the effects of concentration are modelled by Nernst equation.
- Fuel crossover and internal currents. This energy loss results from the waste of fuel passing through the electrolyte, and, to a lesser extent, from electron conduction through electrolyte. The electrolyte should only transport ions through the cell, but a certain amount of fuel diffusion and electron flow will always be possible. The fuel loss and internal currents are small, and their effect is usually not very important. However, it does have a marked effect on the OCP of low-temperature cells.⁷

2.4.1 Activation losses

Butler-Volmer equation represents a standard model that describes the relation between the current density and the electrode over potential of an electrochemical cell at the reactants temperature. In the case of a fuel cell, there are two over potentials: an anodic and a cathodic one

$$i_a = i_{0,a} \left[\exp\left(\frac{\alpha_a^{an} F}{RT} \eta_a\right) - \exp\left(\frac{-\alpha_c^{an} F}{RT} \eta_a\right) \right] \quad (34)$$

$$i_c = i_{0,c} \left[\exp\left(\frac{\alpha_a^{cat} F}{RT} \eta_c\right) - \exp\left(\frac{-\alpha_c^{cat} F}{RT} \eta_c\right) \right] \quad (35)$$

α_a^{an} , α_c^{an} , α_a^{cat} , and α_c^{cat} are the anodic and cathodic transfer coefficients respectively. They are defined as follows

$$\alpha_a^{an} = (1 - \beta) \eta_{el,a} \quad (36)$$

$$\alpha_c^{an} = \beta \eta_{el,a} \quad (37)$$

$$\alpha_a^{cat} = (1 - \beta) \eta_{el,c} \quad (38)$$

$$\alpha_c^{cat} = \beta \eta_{el,c} \quad (39)$$

where:

- β factor contained in equations 36, 37, 38 and 39 is the symmetry factor, and it expresses a fraction of the activation energy, so it can assume values between 0 and 1. The experimental values of β are always really close to 0.5, so that

$$\alpha_a^{an} = \alpha_c^{an} = \alpha^{an} \quad (40)$$

$$\alpha_a^{cat} = \alpha_c^{cat} = \alpha^{cat} \quad (41)$$

- $\eta_{el,a}$ and $\eta_{el,cat}$ represent the number of exchanged electrons in the rate-determining step at the anodic and cathodic site respectively;

- $i_{0,a}$ and $i_{0,c}$ are the exchange current densities, anodic and cathodic respectively;
- η_a and η_c are the anodic and cathodic over potentials respectively.

Thus, anodic and cathodic over potentials can be explicitly expressed as a function of current density

$$\eta_a = \frac{RT}{\alpha^{an}F} \sinh^{-1} \left(\frac{i}{2i_{0,a}} \right) \quad (42)$$

$$\eta_c = \frac{RT}{\alpha^{cat}F} \sinh^{-1} \left(\frac{i}{2i_{0,c}} \right) \quad (43)$$

Often, as in the case of fuel cells, a reduced form of Butler-Volmer can be used. When the value of anodic over potential is high and greater than 0, the first exponential of equation 34 is much greater than the second one, so equation 34 can be written in the form

$$i = i_{0,a} \exp \left(\frac{\alpha^{an}F}{RT} \eta_a \right) \quad (44)$$

The same reasoning can be applied to the cathode. When the value of cathodic over potential is high and lower than 0, the second exponential of equation 35 is much greater than the first one, so equation 35 can be written in the form

$$i = i_{0,c} \exp \left(\frac{\alpha^{cat}F}{RT} \eta_c \right) \quad (45)$$

Equations 44 and 45 are also known as Tafel equation, used for the evaluation of the over potential of electrodes involved in electrochemical reactions.

Tafel equation can also be written expliciting the over potential

$$\eta_{a/c} = \frac{RT}{\alpha^{an/cat}F} \ln \left(\frac{i}{i_{0,a/c}} \right) \quad (46)$$

that is the most useful form, since it can express the activation losses as a function of current density.⁸

2.4.2 Ohmic losses

The losses due to the electrical resistance of the electrodes, and the resistance to the flow of ions in the electrolyte, are the simplest to understand and to model, the size of the voltage drop is simply proportional to the current, that is

$$V = RI \quad (47)$$

Equation 47 is known as the first Ohm's law, this the reason why this type of loss is called Ohmic.

In most fuel cells the resistance is mainly caused by the electrolyte, though the cell interconnects can also be important.

To be consistent with the other equations for voltage loss, the equation should be expressed in terms of current density. To do this it is necessary to introduce the idea of the resistance corresponding to 1 cm² of the cell, which is called the area-specific resistance or ASR. The equation for the voltage drop then becomes

$$\eta_{ohm} = i \sum_j r_j \quad (48)$$

The term r_j represents the ASR of the j -th element (cathode, anode, electrolyte, interconnects, etc.), and it is expressed as

$$r_j = \rho_j t_j \quad (49)$$

where:

- ρ_j is the resistivity of the j -th component $\left[\frac{\Omega\text{cm}^2}{\text{cm}}\right]$;
- t_j is the thickness of the j -th component [cm].

Three ways of reducing the internal resistance of the cell are as follows

- the use of electrodes with the highest possible conductivity;
- good design and use of appropriate materials for the cell interconnects;
- making the electrolyte as thin as possible.⁸

2.4.3 Mass transport or concentration losses

The simplified equation of concentration losses is

$$\eta_{diff} = \frac{RT}{nF} \ln \frac{c_0}{c_\infty} \quad (50)$$

with c_∞ as the reactant concentration before the diffusion layer and c_0 as the reactant concentration in the reaction zone. According to Fick's first law of diffusion, the current density is given by

$$i = \frac{nFD(c_\infty - c_0)}{\delta} \quad (51)$$

where:

- n is the number of electrons participating in the reaction;
- D is the diffusion coefficient of the reactants;
- δ is the diffusion layer thickness.

The current density corresponding to a maximum reactant concentration on the electrode is defined as limiting current density

$$i_l = \frac{nFDc_\infty}{\delta} \quad (52)$$

Combining equations 51 and 52

$$\frac{i}{i_l} = \frac{(c_\infty - c_0)}{c_\infty} \quad (53)$$

and from equation 50

$$\eta_{diff} = \frac{RT}{nF} \ln \left(1 - \frac{i}{i_l} \right) \quad (54)$$

that is a negative quantity. The final expression is⁸

$$\eta_{diff} = \frac{RT}{nF} \ln \left(1 - \frac{i\delta}{nFDc_\infty} \right) \quad (55)$$

2.4.4 Fuel crossover and internal currents

Although the electrolyte of a fuel cell would have been chosen for its ion conducting properties, it will always be able to support very small amounts of electron conduction. Probably more important in a practical fuel cell is that some fuel will diffuse from the anode through the electrolyte to the cathode. Here, because of the catalyst, it will react directly with the oxygen, producing no current from the cell. This small amount of wasted fuel is known as fuel crossover. These two effects (fuel crossover and internal currents) are essentially equivalent. The crossing over of one hydrogen molecule from anode to cathode where it reacts, wasting two electrons, amounts to exactly the same as two electrons crossing from anode to cathode internally, rather than as an external circuit. The flow of fuel and electrons will be small, typically the equivalent of only a few mAcm⁻². In terms of energy loss this irreversibility is not very important. However, in low-temperature cells it does cause a very noticeable voltage drop at open circuit: because of the internal current density, the cell current density is not zero, even if the cell is open circuit. This can cause a large deviation from the reversible voltage, due to the very steep initial fall in voltage that affects some type of fuel cells. The steepness of the curve also explains another observation about low-temperature fuel cells, which is that the OCP is highly variable.

The equivalence of the fuel crossover and the internal currents on the open circuits is an approximation but is quite a fair one in the case of hydrogen fuel cells where the cathode activation overvoltage dominates.

2.4.5 Combining the irreversibilities

It is useful to construct an equation that brings together all the losses described. The following equation expresses the operating voltage of a fuel cell as a function of current density

$$V = E - \eta_{act} - \eta_{ohm} - \eta_{diff} \quad (56)$$

A very similar behaviour characterizes the electrolytic cells too. Since the sign of the current is the opposite in this case, every voltage drop will increase the voltage with reference to the OCP, as shown in Figure 4.

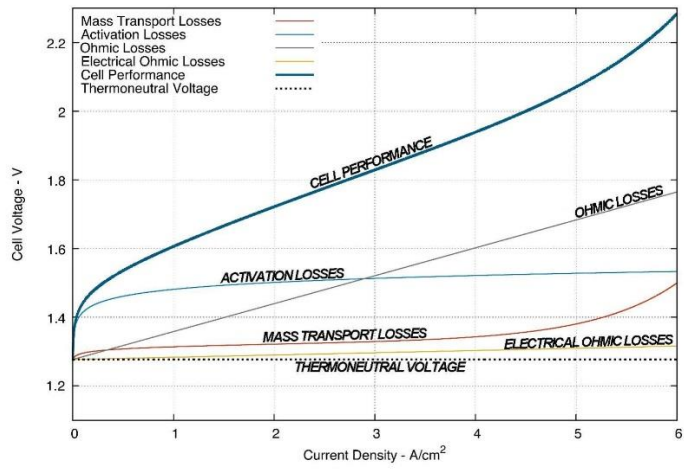


Figure 4 - Typical polarization curve of an electrolytic cell

3 Fuel cell technologies

Fuel cells are efficient and clean devices to electrochemically convert the chemical energy of fuels such as hydrogen, natural gas, methanol, ethanol and hydrocarbons to electric energy with significantly high efficiency and much lower greenhouse-gas emission as compared to well-established internal combustion engine technologies. Thus, fuel cells are regarded as the most promising energy-conversion strategies for the sustainable energy development. Fuel cell technologies can be categorized according to the nature of the electrolytes, including low-temperature proton-exchange membrane fuel cells (PEMFCs), alkaline fuel cells (AFCs), phosphoric acid fuel cells (PAFCs) to high-temperature molten-carbonate fuel cells (MCFCs) and solid-oxide fuel cells (SOFCs). Operating temperatures and ionic-transfer processes of fuel cells are determined by the nature of the electrolytes. As shown in Figure 5, in general, increasing operation temperature will increase the efficiency and decrease the materials cost, while the system complexity and cell and stack fabrication costs increase. The high efficiency of MCFCs and SOFCs is also due to the high quality of heat generated, which can be used for hot-water supply or internal system use. In the case of AFCs, PAFCs and MCFCs, the alkaline, phosphoric acid and molten-carbonate electrolytes are highly corrosive, which significantly limits their commercial viability and competitiveness. PEMFCs and SOFCs are considered to be the most promising and competitive in the future energy-conversion technology sectors.⁹

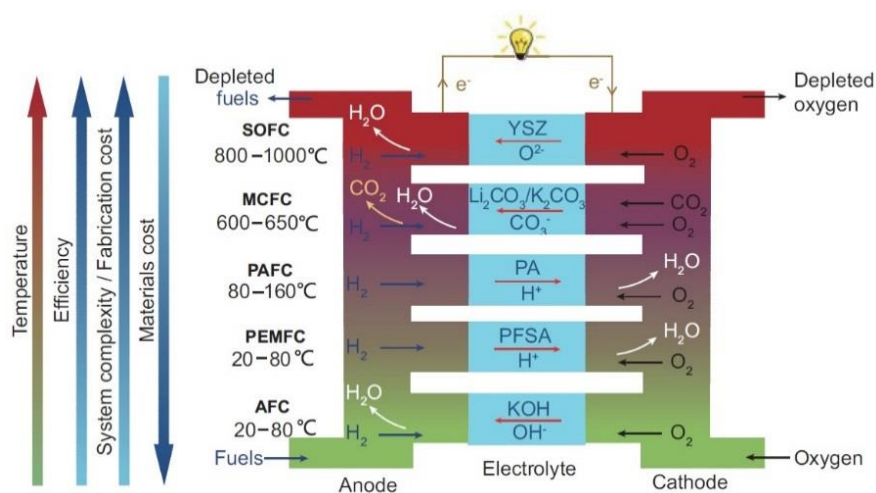


Figure 5 - Fuel cell types, showing the general trend of their features

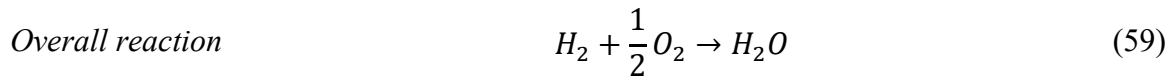
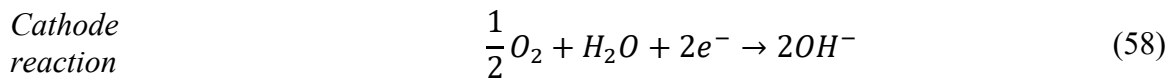
3.1 Low temperature fuel cells

Low temperature fuel cells are generally used to provide power for vehicles, portable devices, spatial applications and small stationary systems. They usually operate in a range of temperature between 40 °C and 150 °C although there is the desire to increase the operating temperature in order to mitigate the poisoning effects of carbon monoxide.¹⁰

3.1.1 Alkaline fuel cells

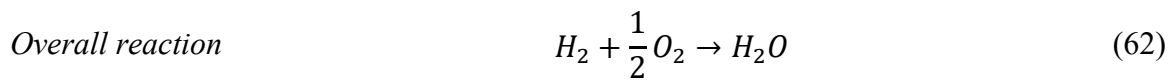
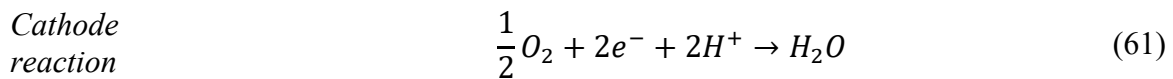
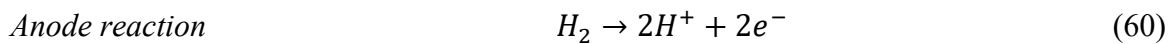
The alkaline fuel cell was the first fuel cell technology to be put into practical service and made the generation of electricity from hydrogen feasible. However, despite its early success and leadership role in fuel cell technology, AFCs have fallen out eclipsed by the rapid development of the PEMFCs as the technology of choice for vehicular applications.

AFCs use an aqueous solution of potassium hydroxide as the electrolyte, with typical concentrations of about 30%. The overall chemical reactions are given by¹¹



3.1.2 Proton exchange membrane fuel cells

A PEM fuel cell is an electrochemical cell that is fed with hydrogen, which is oxidized at the anode, and oxygen that is reduced at the cathode. The protons released during the oxidation of hydrogen are conducted through the proton exchange membrane to the cathode. Since the membrane is not electrically conductive, the electrons released from the hydrogen travel along the electrical detour provided and an electrical current is provided.¹²



3.1.3 Phosphoric acid fuel cells

The PAFC works in a similar fashion to the PEM fuel cell. The PAFC uses a proton-conducting electrolyte, and the reactions occurring on the anode and cathode are the same of PEM fuel cells. In the PAFC, the electrochemical reactions take place on highly dispersed electrocatalyst particles supported on carbon black. As with the PEM fuel cells, platinum or Pt alloys are used as the catalyst at both electrodes. The electrolyte is an organic acid, concentrated phosphoric acid (100%) which, like membranes in the PEM cells, will conduct protons.⁷

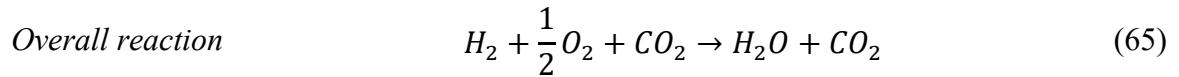
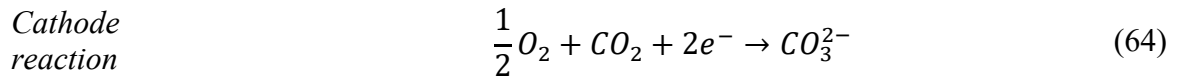
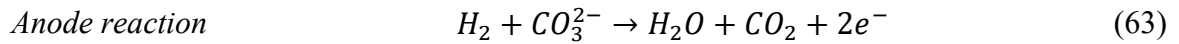
3.2 Medium and high temperature fuel cells

Increasing the operating temperature brings some advantages. First of all, the electrochemical reactions proceed quicker showing lower activation voltage losses, so that noble metal catalysts are often not needed. Moreover, the high temperature of the exit gases means that there is heat available from the cell that can be exploited in different ways. Molten carbonate fuel cells and solid oxide fuel cells are two examples of medium and high temperature fuel cells respectively.

3.2.1 Molten carbonate fuel cells

The electrolyte of the molten carbonate fuel cell is a molten mixture of alkali metal carbonates. At the operating temperature of 600-700 °C the alkali carbonates form a highly conductive molten salt, with carbonate ions providing ionic conduction. Unlike all the other fuel cells, carbon dioxide needs to be supplied to the cathode as well as oxygen, and this becomes converted to carbonate ions, which provide the means of ion transfer

between the cathode and the anode. At the anode, the carbonate ions are converted back into carbon dioxide. The electrochemical reactions of the MCFC are therefore⁷



3.2.2 Solid oxide fuel cells

The SOFCs are similar to the MCFCs in that a negatively charged ion is transferred from the cathode through the electrolyte to the anode. Until recently, SOFCs have all been based on an electrolyte of zirconia stabilized with the addition of a small percentage of yttria. Above a temperature of 800 °C, zirconia becomes a conductor of oxygen ions, and typically the state of the art zirconia-based SOFC operates between 800 and 1100 °C. This is the highest operating temperature of all fuel cells, which presents both challenges and opportunities.⁷ SOFC technology is better explained in following sections.

4 Solid oxide fuel cells

Solid oxide fuel cells are electrochemical devices that produce electrical energy directly from a fuel. Fuel cells are generally classified according to the electrolyte used and/or operating temperature: SOFCs involve a solid oxide electrolyte (usually yttria-stabilized zirconia, a ceramic material) and operates between 800 and 1100 °C.

SOFCs are in principle simpler than all the other fuel cell systems, as only two phases (gas and solid) are required. Both hydrogen and carbon monoxide can act as fuels in SOFCs, as shown in Figure 6.

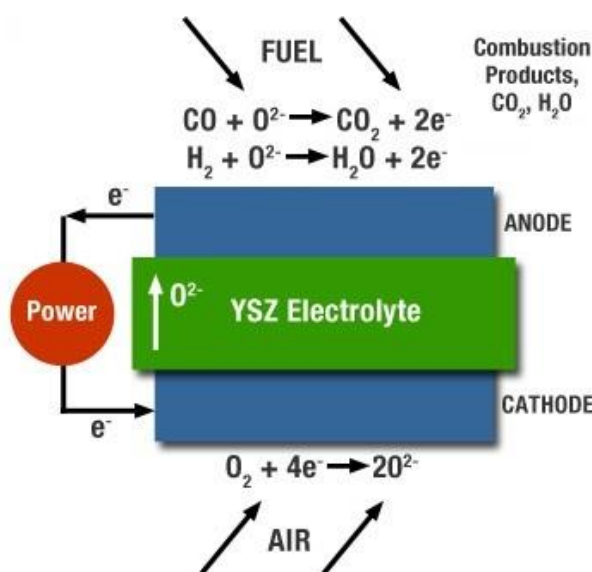


Figure 6 - Operation diagram of a SOFC

A basic SOFC consists of an anode, an electrolyte and a cathode. Driven by the differences in oxygen chemical potential between fuel and air compartments of the cell, oxygen ions migrate through the electrolyte to the anode where they are consumed by oxidation of fuels. Thus, the electrolyte must be dense to separate the air from the fuel, must possess high oxygen ionic conductivity and must be chemically and structurally stable over a wide range of oxygen partial pressure and temperatures. On the other hand, the anode must be porous, electrocatalytically active for the fuel oxidation reaction and chemically and thermally compatible with the electrolyte and interconnect. The cathode is the material where pure oxygen or oxygen from air, combining electrons externally from the cell, is reduced to oxygen ions.

At the cathode side, the oxygen reduction reaction occurs, that in Kröger-Vink notation is written as follows:



At the anode side occurs the fuel oxidation.



Thus, the overall reaction:



From equations 66 and 67, it is possible to understand that a negatively charged ion (O^{2-}) is transferred from the cathode through the electrolyte to the anode. Consequently, product water is formed at the anode.³

4.1 Electrolyte

Zirconia doped with 8 to 10 moles % yttria (yttria-stabilized zirconia (YSZ)) is still the most effective electrolyte for the high temperature SOFC. The ability to conduct O^{2-} ions is brought about by the fluorite crystal structure of zirconia in which some of the Zr^{4+} ions are replaced with Y^{3+} ions. When this ion exchange occurs, a number of oxide-ion sites become vacant because of three O^{2-} ions replacing four O^{2-} ions. Oxide-ion transport occurs between vacancies located at tetrahedral sites in the perovskite lattice.

The ionic conductivity of YSZ (0.02 Scm^{-1} at $800 \text{ }^\circ\text{C}$ and 0.1 Scm^{-1} at $1000 \text{ }^\circ\text{C}$) is comparable with that of liquid electrolytes, and it can be made very thin ($\sim 20 \text{ }\mu\text{m}$) ensuring that the ohmic losses in the SOFC is comparable with other fuel cell types.

Zirconia-based electrolytes are suitable for SOFCs because they exhibit pure anionic conductivity. Some materials show higher oxygen ion conductivities than YSZ but they are less stable at low oxygen partial pressures as found at the anode of the SOFC. This gives rise to defect oxide formation and increased electronic conductivity and thus internal electric currents, which lower the cell potential.⁷

4.2 Anode

The anode of state-of-art SOFCs is a cermet made of metallic nickel and an YSZ skeleton. The zirconia serves to inhibit sintering of the metal particles and provides a thermal expansion coefficient (TEC) comparable to that of the electrolyte. The anode has a high porosity (20-40 %) so that mass transport of reactant and product gases is not inhibited. Often, a small amount of ceria is added to the anode cermet. This improves the tolerance of the anodes to temperature cycling and redox.

In novel ceramic anodes, there is mixed conductivity for both electrons and oxygen ions. They can provide a means of extending the three-phase boundary between reactant, anode and electrolyte, as shown in Figure 7.⁷

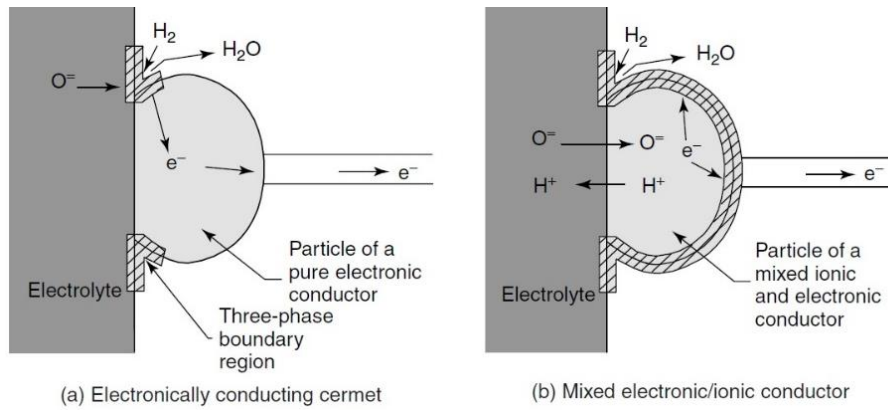


Figure 7 - Comparison of the three-phase boundary regions of different SOFC anode materials

4.3 Cathode

Similar to the anode, the cathode is a porous structure that must allow rapid mass transport of reactant and product gases. Strontium-doped lanthanum manganite, a p-type semiconductor, is most commonly used for the cathode material. Although adequate for most SOFCs, other material may be used, particularly attractive being p-type conducting perovskite structures that exhibit mixed ionic and electronic conductivity. This is especially important for lower-temperature operation since the polarization of the cathode increases significantly as the SOFC temperature is lowered. It is in cells operating at around 650 °C that the advantages of using mixed conducting oxides become apparent.⁷

4.3.1 LSM

Lanthanum strontium manganite (LSM, $\text{La}_{1-x}\text{Sr}_x\text{MnO}_{3-\delta}$) is one of the most common material used as cathode for oxygen reduction reactions in solid oxide fuel cells. LSM is a good electronic conductor, has high stability with yttria stabilized zirconia electrolyte and high electrochemical activity for the oxygen reduction at high temperatures. Its electronic conductivity is in the range of 200 to 300 Scm^{-1} at 900 °C and stable with YSZ up to 1200 °C. However, the oxygen ion conductivity of LSM materials is very low (10^{-7}Scm^{-1} at 900 °C), which seriously limits the use of LSM cathodes in the development of intermediate temperature SOFC.¹³

Strontium-substituted lanthanum manganite belongs to ABO_3 perovskite oxide family. Ideal perovskite crystallizes in cubic close-packed lattice structure. Figure 8 shows the crystal structure of LSM.

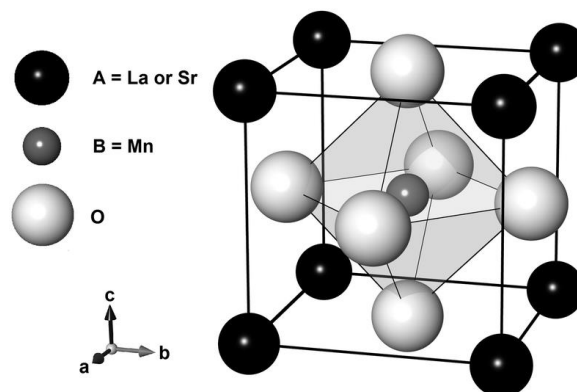


Figure 8 - Crystal structure of LSM

The larger rare earth ions occupy A-sites and the transition metal ions occupy the B-sites. Both the electrical conductivity and catalytic activity of lanthanum is substituted partially with strontium. The stability of the perovskite oxide, in general, increases with the size of A-site cations.³

4.3.2 LSCF

Lanthanum strontium cobalt ferrite (LSCF, $\text{La}_{1-x}\text{Sr}_x\text{Co}_{1-y}\text{Fe}_y\text{O}_{3-\delta}$) is the best known mixed ionic and electronic conducting perovskite and is one of the most investigated MIEC cathodes for intermediate temperature SOFCs due to its high electrical conductivity, high oxygen exchange coefficient and ionic conductivity. The excellent MIEC properties of LSCF imply that the oxygen reduction reaction would occur in the electrode bulk, away from the three-phase boundary. However, LSCF is highly reactive to YSZ electrolyte. To mitigate the reactivity problem, gadolinium-doped ceria is usually used as the electrolyte or as diffusion barrier in YSZ electrolyte system.¹

In LSCF perovskite structure lanthanum and strontium ions occupy the A-sites, while B-sites are occupied by cobalt and iron ions.

4.3.3 BSCF

Barium strontium cobalt ferrite (BSCF, $\text{Ba}_{1-y}\text{Sr}_y\text{Co}_{1-x}\text{Fe}_x\text{O}_{3-\delta}$) is an excellent mixed ionic and electronic conductor and has an excellent electrocatalytic activity for oxygen reduction reaction at reduced temperatures. However, its thermal expansion coefficient (TEC) is substantially higher than the TEC value of the YSZ or GDC electrolytes. BSCF is also chemically incompatible with YSZ at temperatures higher than 800 °C: the reaction leads to the formation of highly resistive phases at the cathode/electrolyte interface, impeding the transport of oxygen ions. Despite its high ionic conductivity, BSCF has low electronic conductivity (30 Scm^{-1} at 800 °C), it could lead to a significant increase in the contact resistance between the current collector and the electrode, resulting in the increase in the electrode polarization losses.¹⁴

4.3.4 NBCaC

Neodymium barium calcium cobaltite (NBCaC, $\text{NdBa}_{1-x}\text{Ca}_x\text{Co}_2\text{O}_{5-\delta}$) is a recently studied material as SOFC cathode, pertaining to a class of double-perovskite oxides. It comes from neodymium barium cobaltite (NBC) doped with Ca in A site.¹⁵ Figure 9 shows the crystal structure of NBCaC.

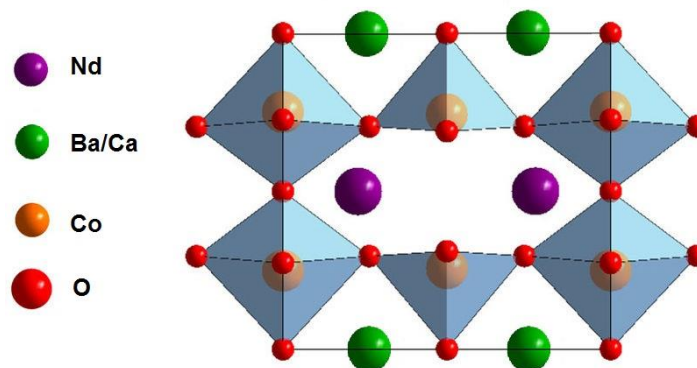


Figure 9 - Crystal structure of NBCaC

NBCaC has been found to present excellent electrochemical performance and stability under operating conditions in both air and CO_2 containing atmosphere. Zhang et al.

intensively tested this material as oxygen electrode for solid oxide cells and reported an extremely high peak power density of 2114 mWcm⁻² measured at 600 °C.¹⁶

4.3.5 Composite cathodes

Composite cathodes consist of materials exhibiting high ionic conductivity and high electronic conductivity at lower temperatures.¹⁷ In this way, the three phase boundary for the oxygen reduction reaction is extended from the cathode/electrolyte interface to the entire cathode bulk, improving the cell performances. Moreover, compare to pristine cathodes, composite cathodes have a thermal expansion coefficient that is closer to the one of the electrolytes. This is fundamental to improve the mechanical strength of the cell and to avoid the formation of mechanical stresses that could lead to some cracks. Another advantage of using composite cathodes is their better chemical stability.¹⁸ In Table 3 are briefly reported the electrochemical properties of the investigated materials found in literature.

Material	Ionic conductivity [Scm ⁻¹]	Electronic conductivity [Scm ⁻¹]	Thermal expansion coefficient [10 ⁻⁶ K ⁻¹]	Reference temperature [°C]
LSM	5.93·10 ^{-7*} 3	180 ¹⁹	12.0 ³	800
LSCF	0.001 ²⁰	300 ²⁰	17.5 ²¹	750
BSCF	0.018**22	30 ²³	24.3 ²³	700
NBCaC***	-	-	-	-
YSZ	0.02 ⁷	-	10.3 ³	800
GDC	0.1 ²⁴	-	12.5 ²⁵	800

* The value has been measured at 900 °C instead of 800 °C. So the ionic conductivity at 800 °C is expected to be even lower

** The value has been measured at 700 °C instead of 750 °C. So the ionic conductivity at 750 °C is expected to be a little larger

*** There are very few publications about NBCaC, so it is very difficult to find its electrochemical properties

Table 3 - Electrochemical and mechanical properties of the investigated materials

5 Experimental

5.1 Samples fabrication

The cells investigated are electrolyte supported half-cells. A three-electrodes half-cell setup was used for the electrochemical measurement: the oxygen electrode was applied on one side of the electrolyte while the reference and the counter electrodes were applied on the other side.²⁶ The three-electrodes half-cell setup is schematically represented in Figure 10.

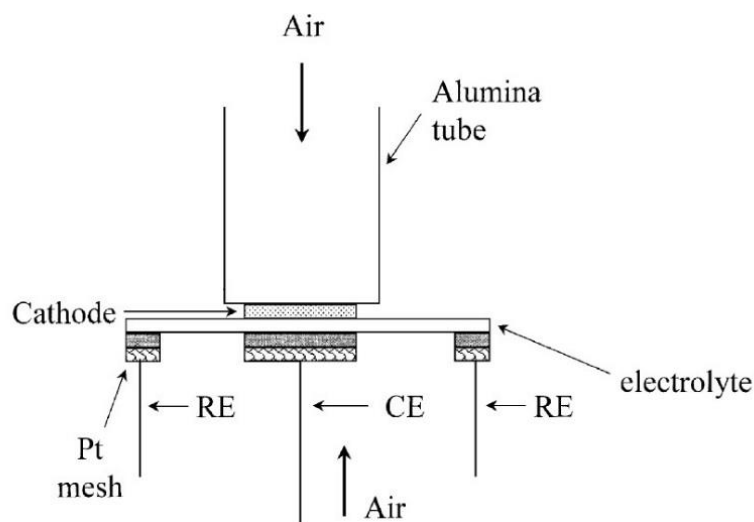


Figure 10 - Three-electrodes half-cell setup

Zirconia electrolyte discs were prepared from 8 mol % Y_2O_3 - ZrO_2 powder. 1,5 g of yttria-stabilized zirconia powder were weighted, put into a mould and by die pressing (Figure 11) submitted at 4 MPa of pressure. After removing the fragile discs from the mould, a sintering procedure is required. Therefore, the YSZ electrolyte discs were sintered at 1450 °C in air for 5 hours (Figure 12).



Figure 11 - YSZ electrolyte disc die pressing



Figure 12 - YSZ electrolyte discs before (left) and after (right) sintering procedure

Platinum paste was painted to the electrolyte disk to make the counter and reference electrodes. The counter electrode was symmetrically positioned at the center. The reference electrode was painted as a ring around the counter electrode, as shown in Figure 13. The gap between counter and ring reference electrodes was about 4 mm.¹³ Platinum paste was then sintered at 1100 °C in air for 2 hours.

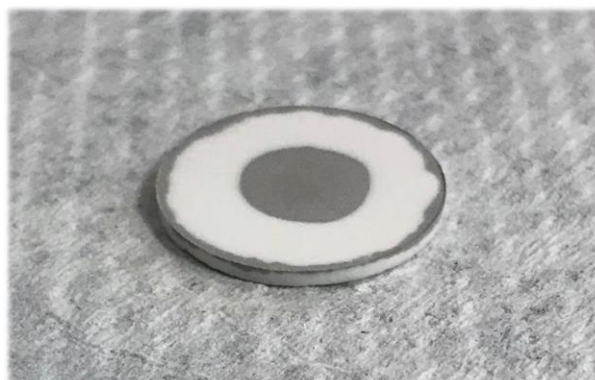


Figure 13 - Reference and counter electrode

On the other side of the electrolyte disc, the working electrode was painted. The working electrode ink was produced dispersing the composite powder in an ink vehicle, in a weight ratio of 3:2.

The composite powder was obtained mixing in a mortar a typical cathode material powder (LSM, LSCF, BSCF or NBCaC) and a typical electrolyte material powder (YSZ or GDC) in a weight ratio of 1:1. In most of the cases, already made powders were used, but in others, such as BSCF and NBCaC, the powder was prepared by the combined citrate and ethylenediaminetetraacetic acid (EDTA) complexing method.

For the BSCF fabrication, the following nitrates were used: $\text{Ba}(\text{NO}_3)_2$, $\text{Sr}(\text{NO}_3)_2$, $\text{Co}(\text{NO}_3)_2 \cdot 6\text{H}_2\text{O}$ and $\text{Fe}(\text{NO}_3)_3 \cdot 9\text{H}_2\text{O}$. The molar ratio of metal ions, citric acid and EDTA was 1:1,5:1.²⁷ Furthermore, for every 0,1 mol of metal ions, 60 ml of ammonia solution were added. The solution was then heated and stirred until a dark gel was observed. The heating process was continued until the gel was burnt completely and became ash. The ash was then completely dried into the oven at 150 °C for one night. The ash was then crushed in order to get a fine powder and then calcined at 1100 °C for 4 hours.²⁸

To prepare NBCac cathode powder, $\text{Nd}(\text{NO}_3)_3 \cdot 6\text{H}_2\text{O}$, $\text{Ba}(\text{NO}_3)_2$, $\text{Ca}(\text{NO}_3)_2$ and $\text{Co}(\text{NO}_3)_2 \cdot 6\text{H}_2\text{O}$ were dissolved in distilled water with ethylene glycol and citric acid added as the chelate agent. The molar ratio of total metal ions, ethylene glycol and citric acid was 1:1.5:3. The solution was stirred and heated at 80 °C for 2 hours, and then vaporized in an oven at 300 °C, followed by calcination in air at 900 °C for 5 hours to form layered perovskite NBCaC.²⁹

The formation of desired perovskite phases was confirmed by X-ray diffraction (XRD).

The ink was then painted on the YSZ electrolyte by slurring coating, as shown in Figure 14, and dried at 100 °C for 2 hours to form the in situ assembled electrode without further pre-sintering. The effective cathode area was 0.5 cm². LSM, LSCF, BSCF or NBCaC, according to the nature of the composite cathode, were painted on the working electrodes as a current collector and then dried at 150 °C for 2 hours without pre-heat-treatment.²⁷ The current collector is a porous layer that covers the oxygen electrode surface to ensure that current is collected from the whole electrode area. In principle, the current collector layer is electrochemically inactive. However, since it covers and fills voids and cracks in the electrode, thus contacting a number of YSZ grains, some little contribution to the TPB is expected.³⁰



Figure 14 - Working electrode application on YSZ electrolyte disc by slurry coating

5.1.1 In-situ vs pre-sintered approach

The most active cathodes for intermediate temperature SOFC belong to mixed ionic and electronic conducting cobaltite-based perovskites (CBP), which show excellent electrocatalytic activity for the O₂ reduction reaction. Unfortunately, CBPS cannot be directly applied on YSZ electrolyte due to their high chemical activity during the high temperature sintering in the traditional cathode fabrication process (pre-sintered). Thus, in order to use CBP cathodes and to avoid the interfacial reaction, a doped ceria barrier layer has to be employed between the cathode and YSZ electrolyte. However, the use of a ceria interlayer in a cell requires additional fabrication steps. This increases the complexity and the cost of the cell, and more importantly increases the risk of the cell degradation and delamination due to incompatibility in chemical and thermal properties between YSZ and ceria interlayer. The presence of a porous ceria layer also leads to an increase of ohmic resistance due to the poor contact at the ceria/YSZ interface to form insulating SrZrO₃. An in-situ assembly process can be used in order to apply CBP cathodes directly on YSZ electrolyte, with no requirement of a GDC interlayer and high temperature sintering steps. The in-situ assembly process significantly reduces the fabrication steps for SOFCs and

the elimination of high temperature sintering avoids the chemical reaction between CBPs and the YSZ electrolyte.²⁷ Figure 15 shows schematically the differences between the two approaches.

The chosen testing temperature is 750 °C, because it is a good compromise between the chemical reactivity of LSCF and YSZ at higher temperatures and the very low catalytic activity of LSM at lower temperatures.²⁷

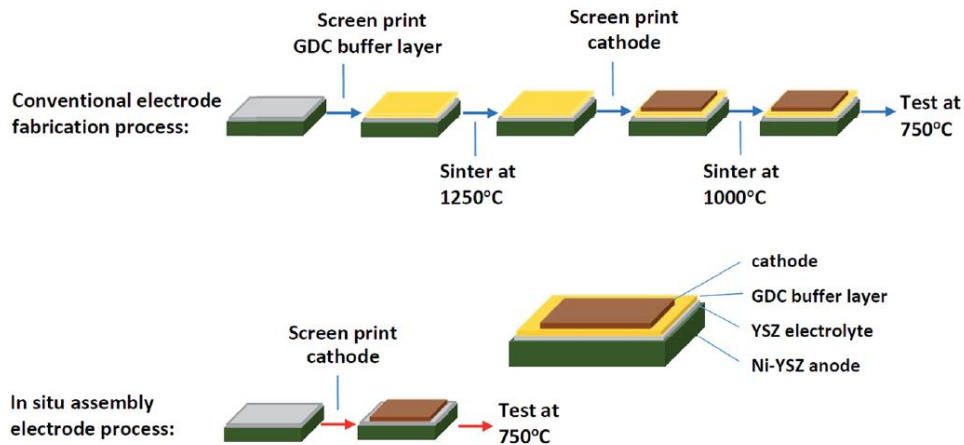


Figure 15 - Pre-sintered vs in-situ approach

This choice leads to the use of YSZ as the electrolyte, despite its lower ionic conductivity compared to GDC, because the latter, in reducing conditions at temperatures above 600 °C, brings to the reduction of Ce^{4+} , forming Ce^{3+} .³¹ Reduction of cerium induces n-type semi conduction in the material, causing an increase in the unit cell volume, which can cause cracks formation in the component. Considering that the aim is to reduce the operating temperature for the SOFC, reaching 600 °C and lower, this should not be a problem in future.

In some of the cases, a thermal compatibility test has been required, to verify if new phases were originated by eventual chemical reactions occurring between the two materials forming the composite oxygen electrode.

5.2 Experimental tests

To carry on the electrochemical analysis, the sample is positioned inside a furnace that can heat the half-cell up to the desired temperature. Each electrode is placed in contact with a platinum mesh, to guarantee an adequate connection, as shown in Figure 16. Air was then directed to the working electrode through an alumina tube.¹³



Figure 16 - Three electrodes setup

5.2.1 Electrochemical impedance spectroscopy

In order to evaluate the performance of the studied half-cells, it is fundamental to measure their impedance. Like resistance, impedance is a measure of the ability of a circuit to resist the flow of electrical current, but unlike resistance, it is not limited by the simplifying properties of an ideal resistor. Electrochemical impedance is usually measured by applying an AC potential to an electrochemical cell and then measuring the current through the cell. It is generally measured applying a small excitation signal. This is done so that the cell's response is pseudo-linear. In a linear (or pseudo-linear) system, the current response to a sinusoidal potential will be a sinusoid at the same frequency but shifted in phase. In a linear system, the response signal, I_t , is shifted in phase (ϕ) and has a different amplitude, I_0 .

$$I_t = I_0 \sin(\omega t + \phi) \quad (69)$$

An expression analogous to Ohm's Law allows us to calculate the impedance of the system as:

$$Z = \frac{E_t}{I_t} = \frac{E_0 \sin(\omega t)}{I_0 \sin(\omega t + \phi)} = Z_0 \frac{\sin(\omega t)}{\sin(\omega t + \phi)} \quad (70)$$

The impedance is therefore expressed in terms of a magnitude, Z_0 , and a phase shift, ϕ . With Eulers relationship

$$\exp(j\phi) = \cos\phi + j\sin\phi \quad (71)$$

it is possible to express the impedance as a complex function

$$Z(\omega) = \frac{E}{I} = Z_0 \exp(j\phi) = Z_0(\cos\phi + j\sin\phi) \quad (72)$$

If the real part is plotted on the X-axis and the imaginary part is plotted on the Y-axis of a chart, it is possible to get a "Nyquist plot". On the Nyquist plot the impedance can be represented as a vector of length $|Z|$. The angle between this vector and the X-axis, is the phase angle ϕ . Nyquist plots have on major shortcoming: it is impossible to tell what frequency was used to record the different points. Electrochemical impedance plots often contain semicircles. The semicircle is characteristic of a single time constant. Another popular presentation method is the Bode plot. The impedance is plotted with log

frequency on the X-axis and both the absolute values of the impedance and the phase-shift on the Y-axis.

Electrochemical impedance spectroscopy (EIS) data is commonly analyzed by fitting it to an equivalent electrical circuit model. Most of the circuit elements in the model are common electrical elements such as resistors, capacitors and inductors. To be useful, the elements in the model should have a basis in the physical electrochemistry of the system. Table 4 lists the common circuit elements, the equation for their current versus voltage relationship, and their impedance.

Component	Current vs Voltage	Impedance
Resistor	$E=IR$	$Z=R$
Capacitor	$E=Ldi/dt$	$Z=j\omega L$
Inductor	$I=CdE/dt$	$Z=1/(j\omega C)$

Table 4 - Impedance of circuit elements

Very few electrochemical cells can be modeled using a single equivalent circuit element. Instead, EIS models usually consist of a number of elements connected together. Both serial and parallel combination of elements occur.

In the studied half-cells, three major contributors to the total impedance can be identified: electrolyte resistance, double layer capacity and charge transfer resistance. Electrolyte resistance is usually a significant factor in the impedance of an electrochemical cell. The resistance of the electrolyte depends on the ionic concentration, type of ions, temperature and the geometry of the area in which current is carried. In a bounded area, A , and length, l , carrying a uniform current, the resistance is defined as

$$R = \rho \frac{l}{A} \quad (73)$$

where ρ is the electrolyte resistivity. The reciprocal of ρ , σ , is more commonly used. σ is the electrolyte ionic conductivity and its relationship with solution resistance is

$$R = \frac{1}{\sigma} \frac{l}{A} \rightarrow \sigma = \frac{l}{RA} \quad (74)$$

Unfortunately, most electrochemical cells do not have uniform current distribution through a definite electrolyte area. The major problem in calculating solution resistance therefore concerns determination of the current flow path and the geometry of the electrolyte that carries the current.

An electrical double layer exists on the interface between an electrode and its surrounding electrolyte. This double layer is formed as ions from the solution “stick on” the electrode surface. The charge electrode is separated from the charged ions. The separation is very small, often on the order of angstroms: charges separated by an insulator form a capacitor. The value of the double layer capacitance depends on many variables: electrode potential, temperature, ionic concentrations, types of ions, oxide layers, electrode roughness and impurity adsorption are all factors.

The charge transfer resistance is formed by a single kinetically-controlled electrochemical reaction. In this case there is no a mixed potential, but rather a single reaction at

equilibrium. Considering a metal substrate in contact with an electrolyte, the metal can electrolytically dissolve into the electrolyte, according to



or more generally



In the forward reaction in the first equation, electrons enter the metal and metal ions diffuse into the electrolyte. Charge is being transferred. This charge transfer reaction has a certain speed. The speed depends on the kind of reaction, the temperature, the concentration of the reaction products and the potential. The general relation between the potential and the current (which is directly related with the number of electrons) is the Butler-Volmer equation. When the overpotential, η , is very small and the electrochemical system is at equilibrium, the expression for the charge transfer resistance changes to

$$R_{ct} = \frac{RT}{nFi_0} \quad (77)$$

From equation 77 the exchange current density can be calculated when R_{ct} is known.

The model used to study the prepared half-cells is the simplified Randles cell. The simplified Randles cell is one of the most common cell models. It includes an electrolyte resistance (R_s), a double layer capacitor (C_{dl}) and a charge transfer (or polarization) resistance (R_{ct} or R_p). The double layer capacitance is in parallel with the charge transfer resistance. The equivalent circuit for a simplified Randles cell is shown in Figure 17a. Figure 17b shows the Nyquist plot for a typical simplified Randles cell.

The Nyquist plot for a simplified Randles cell is always a semicircle. The electrolyte resistance can be found by reading the real axis value at high frequency intercept. This is the intercept near the origin of the plot. The real axis value at the other intercept (low frequency) is the sum of the polarization resistance and the electrolyte resistance.³²

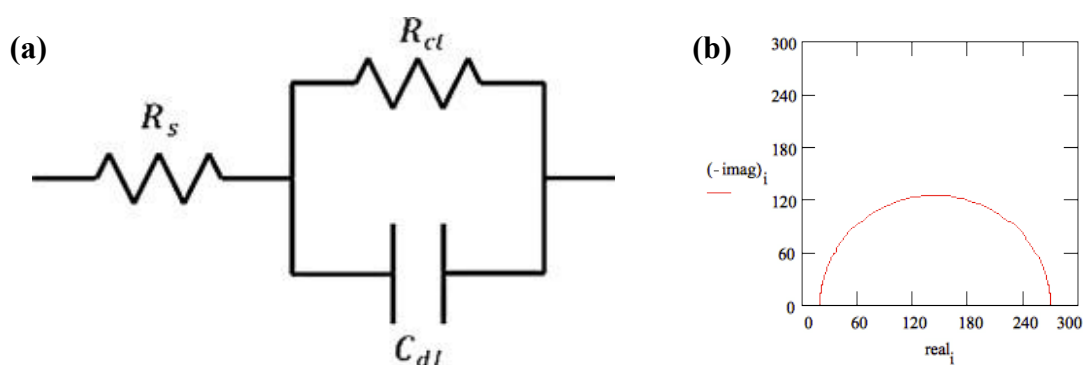


Figure 17 - Simplified Randles cell circuit and relative Nyquist plot

Electrochemical impedance curves were measured in a frequency range of 100 kHz to 0,1 Hz with a signal amplitude of 10 mV under open circuit, before, after and during the polarization phase.

5.2.2 Galvanostatic polarization

Galvanostatic polarization is an experimental technique whereby an electrochemical cell is maintained at a constant current. This technique is generally used to measure corrosion rate, electrochemical reactions, and, in this case, the interface formation between working electrode and YSZ electrolyte. In galvanostatic polarization measurements, the current between working and reference electrodes is controlled, and the potential between the two is automatically adjusted to the value required to maintain the desired current value. In galvanostatic polarization tests, the potential is plotted versus time. Galvanostatic polarization was interrupted time to time to carry out the EIS. The galvanostatic polarization measurements were carried out under cathodic (fuel cell mode) and anodic (electrolysis mode) polarization, at 250 mAcm^{-2} and 500 mAcm^{-2} .

5.2.3 Open circuit potential

In order to evaluate the operating temperature effect on the half-cell performances, the samples were left into the furnace under OCP condition for 12 hours (the typical experiment length). EIS measurements were carried out before and after the OCP treatment.

5.2.4 Interface analysis

The interface between the oxygen electrode and the electrolyte was examined using scanning electron microscopy (SEM). The in-situ applied working electrodes were removed by using adhesive tape, and the elemental distribution on the YSZ electrolyte surface was analyzed by time of flight secondary ion mass spectroscopy using a focused ion beam-SEM (FIB-SEM).

A cross-sectional lamella at the electrode/electrolyte surface was prepared in the FIB-SEM. Microstructure and elemental mapping analysis of the lamella were carried out using high angle annular dark field scanning transmission electron microscopy (HAADF-STEM). In some cases, the oxygen electrodes were removed from the electrolyte surface by ultrasonic treatment in HCl solution, to analyze the YSZ surface.²⁷

6 Results

6.1 LSM

LSM is the first and the most used material for oxygen electrode in SOFC, due to its high chemical stability and its good catalytic activity. Since its negligible ionic conductivity, it is almost never used alone, always mixed with some good ionic conductor. Figure 18 shows the poor performance of the LSM pristine cathode under cathodic polarization.

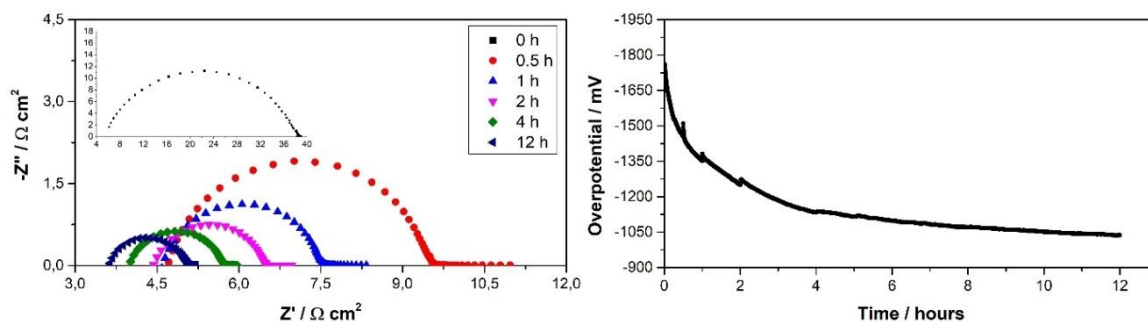


Figure 18 - Impedance and polarization curves of LSM pristine electrode, on YSZ electrolyte under 250 mAcm^{-2} of cathodic current density

The initial R_p value is extremely high, higher than 30 Ωcm^2 . During the whole length of the experiment, it keeps decreasing, accompanied by a slightly decrease of the R_s , signal of the formation of an intimate electrolyte/electrode interface.

6.1.1 LSM/YSZ

LSM is thermally compatible with YSZ at temperature lower than 1150 °C .³³ Under cathodic polarization, LSM/YSZ composite cathode showed a progressive decrease of the polarization resistance for the whole test length, with a final value of 1.8 Ωcm^2 for the 250 mAcm^{-2} polarization (Figure 19), and 1.0 Ωcm^2 for the 500 mAcm^{-2} one (Figure 20). In the first case the ohmic resistance is quite constant, while in the second one it slightly decreases. Probably, because of the temperature, the contact between the Pt mesh on the top of the alumina tube and the current collector of the half-cell improved with time. Such improvement on the cell performance suggests a good interface formation between the electrolyte and the cathode.

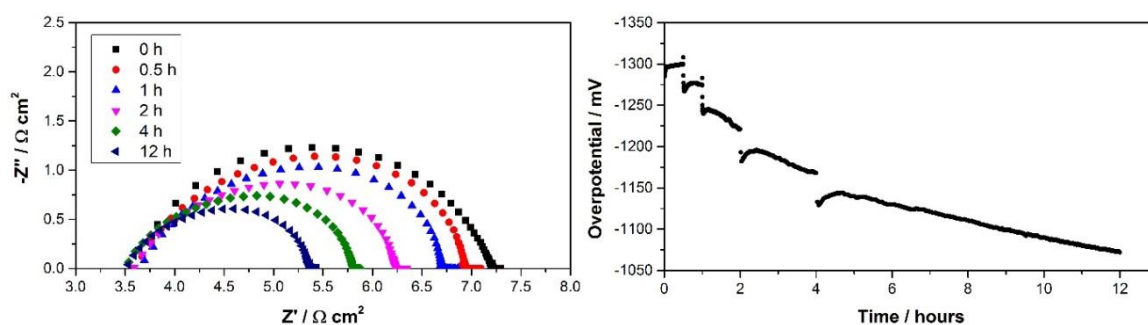


Figure 19 - Impedance and polarization curves of LSM/YSZ composite electrode, on YSZ electrolyte under 250 mAcm^{-2} of cathodic current density

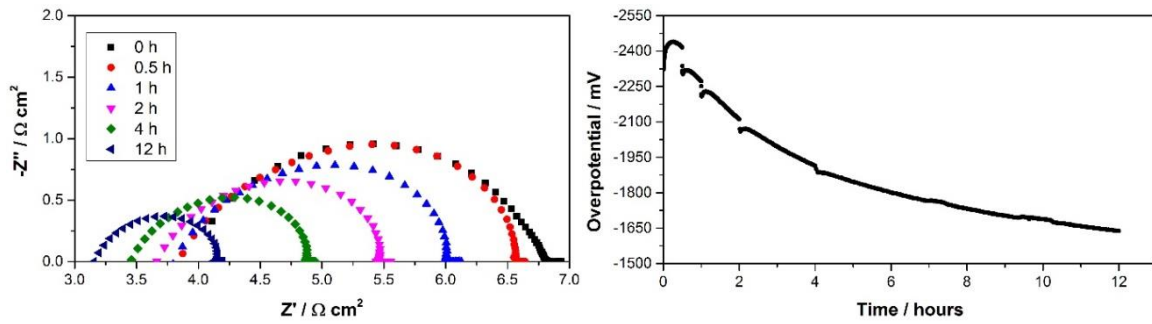


Figure 20 - Impedance and polarization curves of LSM/YSZ composite electrode, on YSZ electrolyte under 500 mAcm^{-2} of cathodic current density

Figure 21 shows the SEM images of the YSZ electrolyte surface after 12 hours of cathodic polarization at different magnifications. The cathode coating was removed by adhesive tape. The particles average size is less than $1 \mu\text{m}$. The bigger particles, highlighted in Figure 21b, are very likely LSM residual particles.

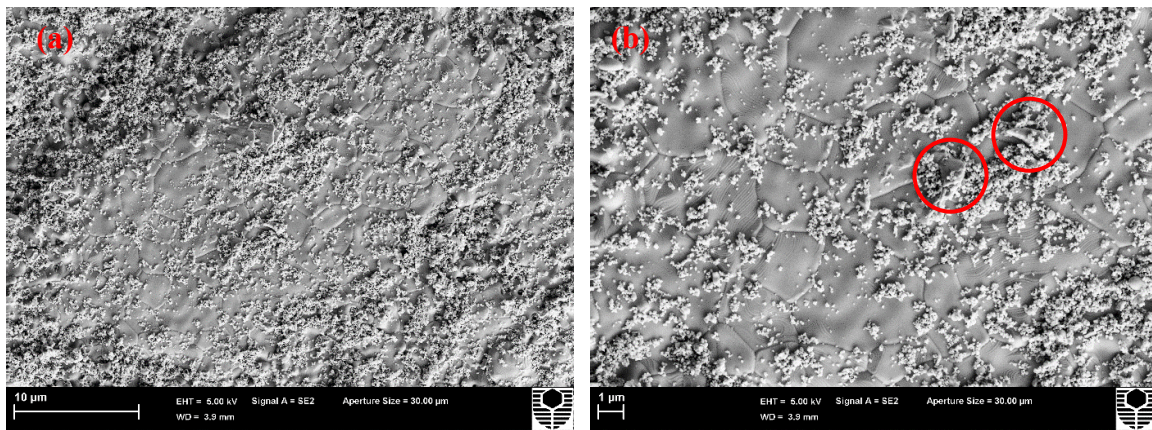


Figure 21 - SEM images of YSZ electrolyte surface after 12 hours of cathodic polarization. Red circles highlight LSM particles

Under anodic polarization, the performance improvement is not so evident. In both cases, the final R_p values are relatively high. Despite a constant R_p reduction, Figure 22 shows a final R_p value higher than $3 \Omega\text{cm}^2$, not as good as the case under cathodic polarization current. Under 500 mAcm^{-2} of anodic current density, as shown in Figure 23, R_s slightly decreased, while R_p was quite constant under the whole test length, with a final value of $2.5 \Omega\text{cm}^2$.

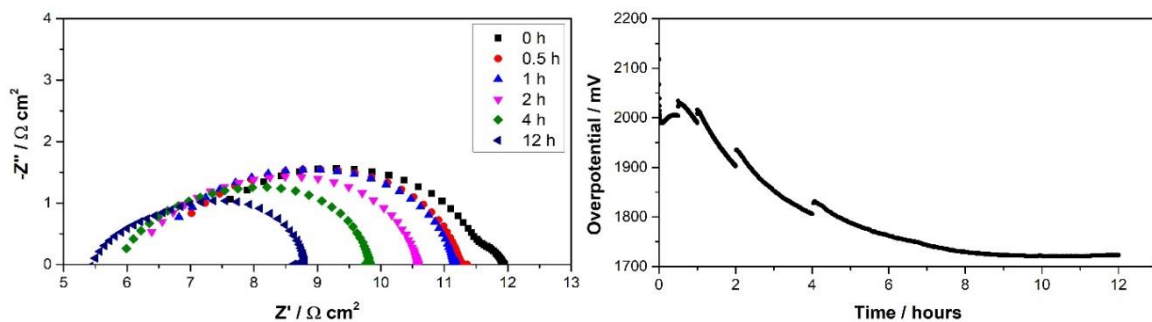


Figure 22 - Impedance and polarization curves of LSM/YSZ composite electrode, on YSZ electrolyte under 250 mAcm^{-2} of anodic current density

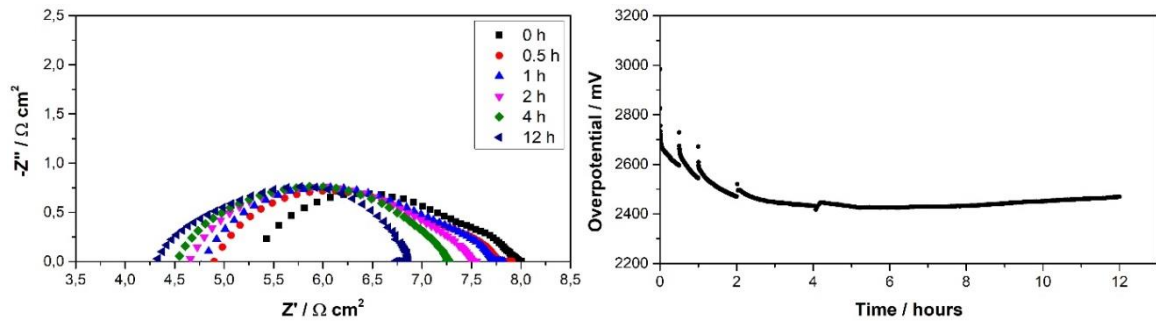


Figure 23 - Impedance and polarization curves of LSM/YSZ composite electrode, on YSZ electrolyte under 500 mAcm^{-2} of anodic current density

The SEM images of the YSZ electrolyte surface after 12 hours of anodic polarization are reported in Figure 24, treated with hydrochloric acid in order to remove the cathodic layer. Despite the acid treatment, lots of YSZ particles were still attached to the electrolyte surface. The concentric lines highlighted in Figure 24b are formations caused by the strain stresses accumulated during YSZ pressing and sintering procedure.

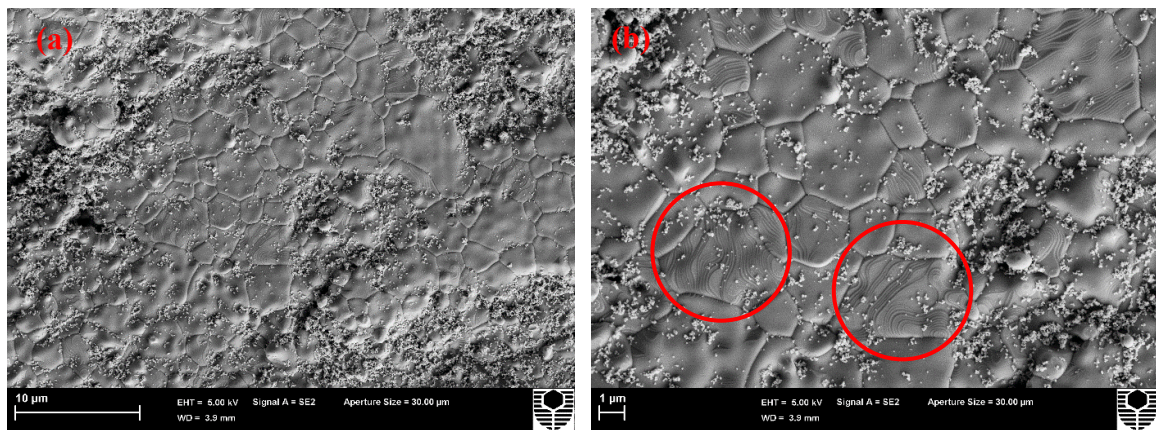


Figure 24 - SEM images of YSZ electrolyte surface after 12 hours of cathodic polarization. Red circles highlight the strain stresses accumulated during the YSZ pressing procedure

Leaving the half-cell under OCP for 12 hours at the testing temperature and measuring the impedance before and after the treatment helps understanding if the temperature has a significant influence on the cell performances.

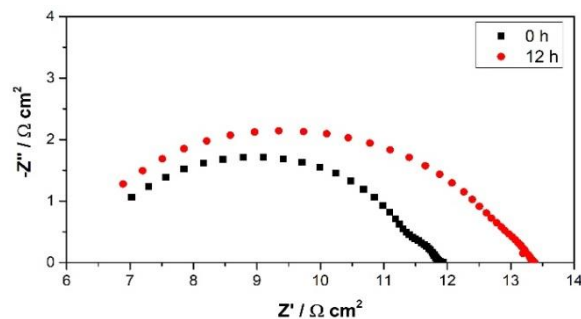


Figure 25 - Impedance and polarization curves of LSM/YSZ composite electrode, on YSZ electrolyte before and after 12 hours of open circuit potential

Figure 25 shows that the heating treatment made the polarization resistance slightly increase, while the electrolyte resistance seems to be rather constant. No positive effects are attributable to the temperature treatment.

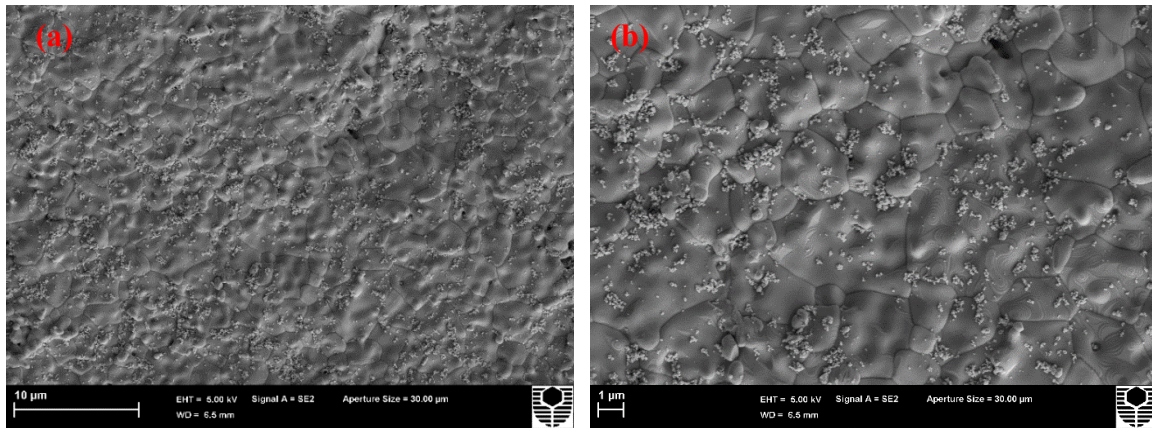


Figure 26 - SEM images of YSZ electrolyte surface after 12 hours of open circuit potential

In Figure 26 are shown the SEM images of the YSZ electrolyte surface after 12 hours of open circuit potential. The cathode was removed by adhesive tape. Compared to Figure 21, the two images are much cleaner. This means that the current flowing through the cell helps to create a stronger contact between the electrolyte and the oxygen electrode.

6.1.2 LSM/GDC

LSM has no thermal compatibility issues with GDC at temperatures as high as 1300 °C.³³ Under 250 mAcm⁻² of cathodic current density, R_p quickly decreased from 0.89 Ωcm² to 0.44 Ωcm² in the first half hour, and then it remained constant, Figure 27. Instead, R_s kept decreasing until the end. Unfortunately, during the 500 mAcm⁻² cathodic test of LSM/GDC composite electrode, the electrochemical station was experiencing some problems interrupting the current for the EIS measurements. So, as shown in Figure 28, has been decided to measure the half-cell impedance just twice, before and after one single 12 hours cathodic polarization, at constant current density. The over potential kept decreasing constantly. Such improvement was mainly due to the electrolyte resistance, with a reduction from 3.1 Ωcm² to 2.3 Ωcm² (about 26 %) while the polarization resistance decreased from 0.9 Ωcm² to 0.7 Ωcm² (about 22 %).

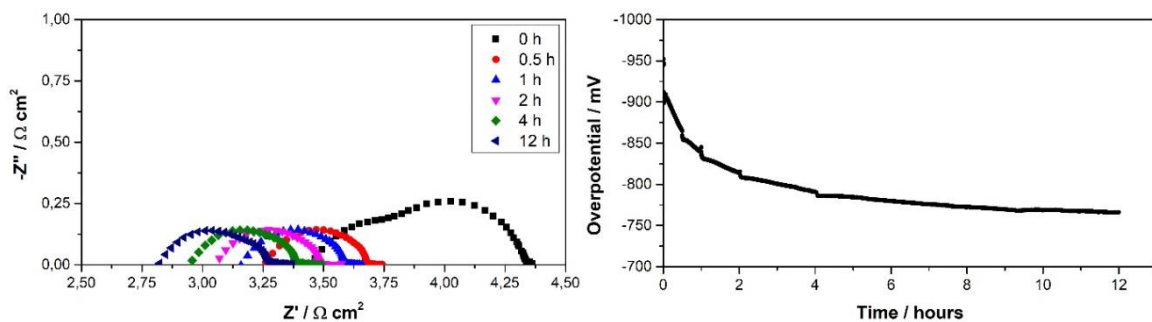


Figure 27 - Impedance and polarization curves of LSM/GDC composite electrode, on YSZ electrolyte under 250 mAcm⁻² of cathodic current density

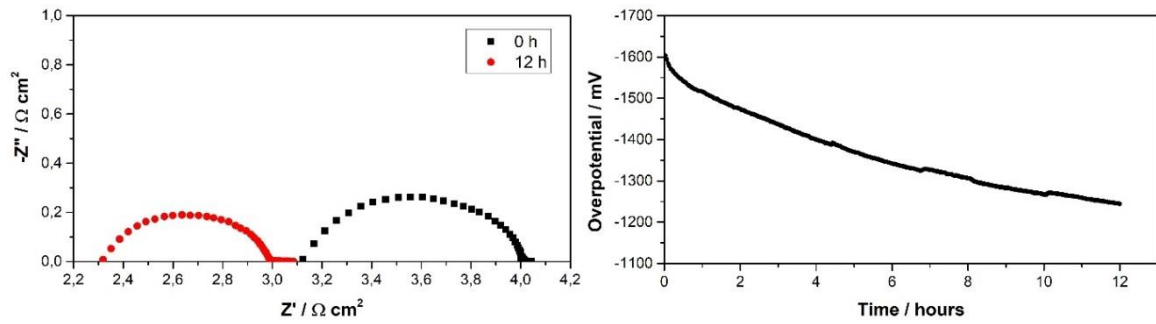


Figure 28 - Impedance and polarization curves of LSM/GDC composite electrode, on YSZ electrolyte under 500 mAcm^{-2} of cathodic current density

Figure 29 shows the SEM images of the YSZ electrolyte surface after 12 hours of cathodic polarization. The cathode was removed by adhesive tape. In this case no particles bigger than $1 \mu\text{m}$ are visible, suggesting a good efficiency of the powder grounding process.

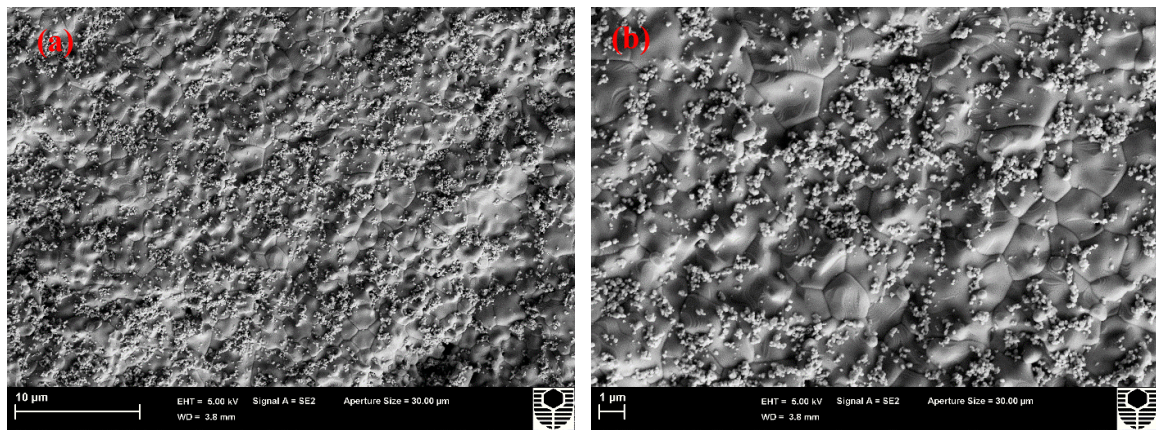


Figure 29 - SEM images of YSZ electrolyte surface after 12 hours of cathodic polarization

LSM/GDC composite electrodes tested under electrolysis mode didn't show good results. In both cases, under 250 mAcm^{-2} (Figure 30) and 500 mAcm^{-2} (Figure 31), the ohmic resistances decreased while the polarization ones almost doubled their initial values. As already suggested by LSM/YSZ testing, anodic polarization gave no positive effects for the LSM composite electrodes activation.

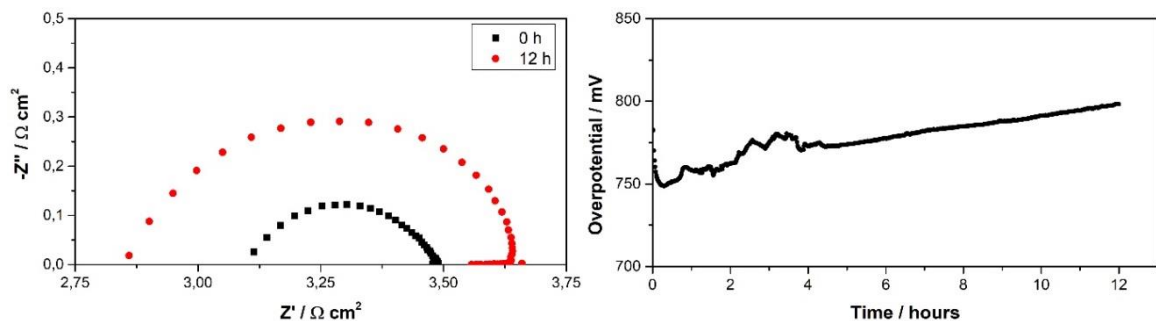


Figure 30 - Impedance and polarization curves of LSM/GDC composite electrode, on YSZ electrolyte under 250 mAcm^{-2} of anodic current density

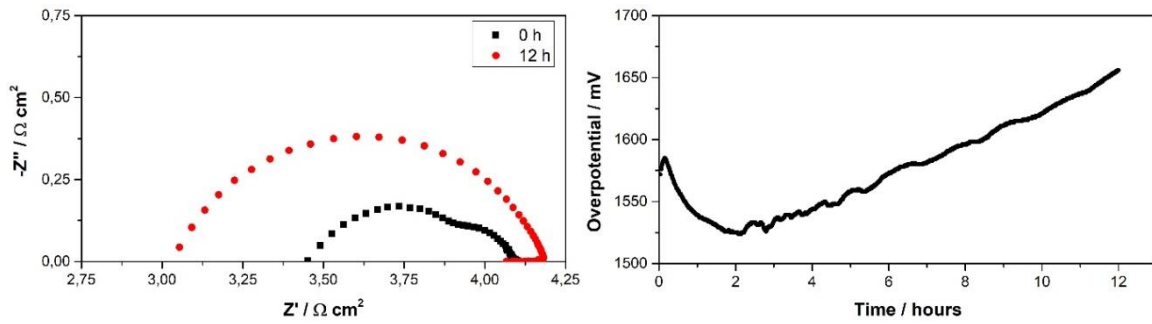


Figure 31 - Impedance and polarization curves of LSM/GDC composite electrode, on YSZ electrolyte under 500 mAcm⁻² of anodic current density

Figure 32 shows the SEM images of the YSZ electrolyte surface after 12 hours of anodic polarization. The cathode was removed by hydrochloric acid treatment. In Figure 32b, it is possible to see some little holes on the YSZ electrolyte surface. These holes are probably due by the air escaping from the YSZ pellet, trapped during the pressing procedure.

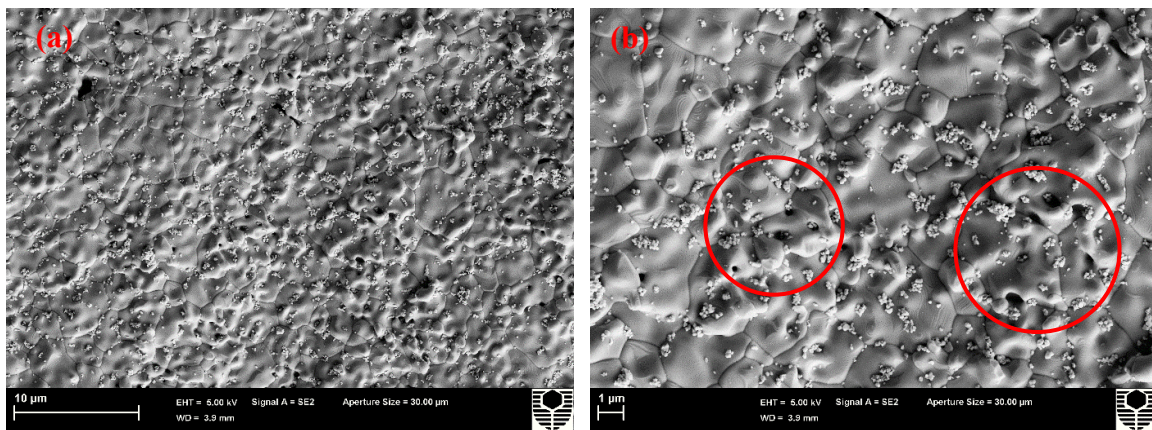


Figure 32 - SEM images of YSZ electrolyte surface after 12 hours of anodic polarization. Red circles highlight the presence of little holes on the YSZ surface

The last test performed on LSM/GDC composite electrode, reported in Figure 33, shows that no positive effects are given by the temperature treatment, in terms of polarization resistance. The electrolyte resistance, instead, decreased significantly. In this way, the overall resistance of the cell remained constant

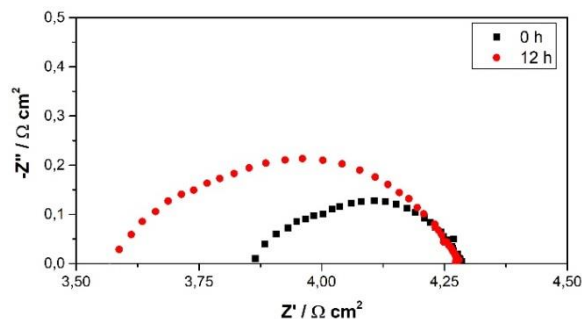


Figure 33 - Impedance and polarization curves of LSM/GDC composite electrode, on YSZ electrolyte before and after 12 hours of open circuit potential

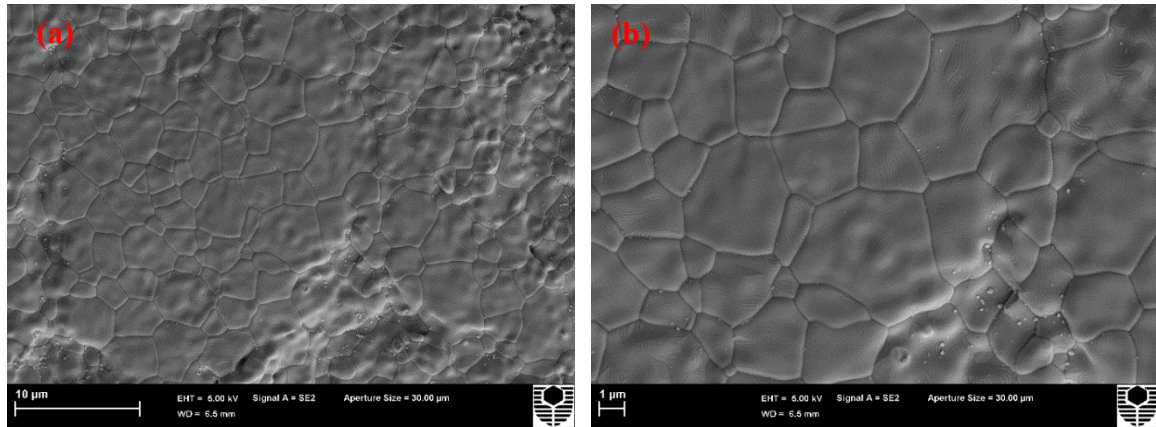


Figure 34 - SEM images of YSZ electrolyte surface after 12 hours of open circuit potential

In Figure 34, are reported the SEM images of the YSZ electrolyte surface after 12 hours of open circuit potential. The cathode layer was removed by hydrochloric acid. In the two images, compared to the polarized cases, there is very little traces of the LSM/GDC layer. This testifies the poor contact between the YSZ and the LSM/GDC composite oxygen electrode.

6.2 LSCF

LSCF is probably the first and the most MIEC material used as oxygen electrode in SOFC. Despite its incredible properties, it easily reacts with YSZ to form a new phase, SrZrO_3 . This is the reason why it is usually used with a doped ceria buffer layer.¹³ However, the goal of this work is to test the performances of several directly assembled composite oxygen electrode, without the use of any buffer layer.

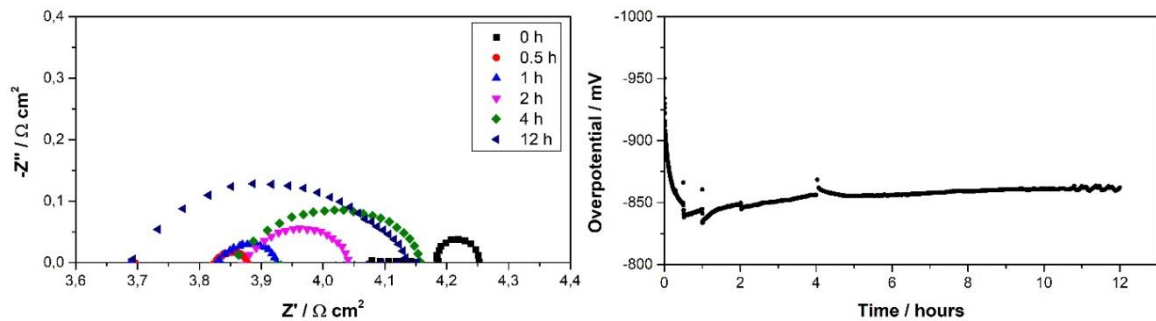


Figure 35 - Impedance and polarization curves of LSCF pristine electrode, on YSZ electrolyte under 250 mAcm^{-2} of cathodic current density

The first test was performed on a LSCF pristine electrode under 250 mAcm^{-2} of cathodic current density. The results of the test are reported in Figure 35. They show very low polarization resistance values for the first half an hour, around $0.5 \text{ } \Omega\text{cm}^2$, and then a constant deterioration, that is probably due to the occurring of the reaction between LSCF and YSZ.

6.2.1 LSCF/YSZ

It is demonstrated that LSCF reacts with YSZ at temperatures higher than $900 \text{ }^\circ\text{C}$.³⁴ However, despite the electrochemical tests were performed at $750 \text{ }^\circ\text{C}$, the results showed a constant rising of the ohmic and polarization resistances, both under cathodic (Figure 36) polarization and anodic (Figure 37) polarization. Although the final values are quite bad, the initial ones are very promising, demonstrating the excellent properties of LSCF.

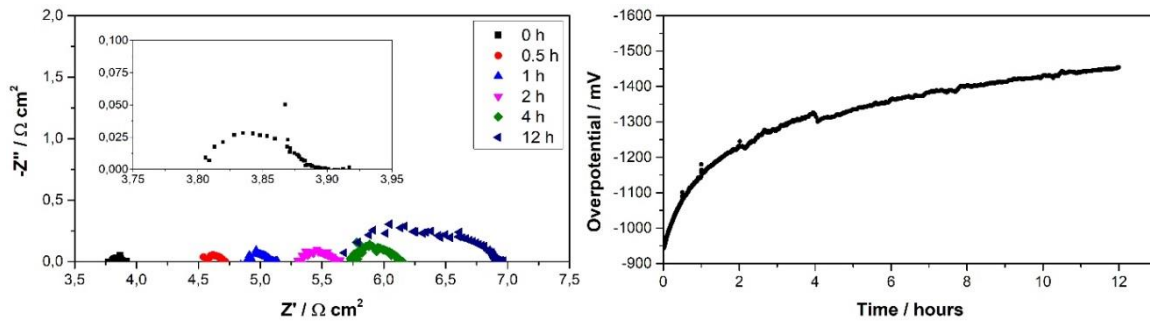


Figure 36 - Impedance and polarization curves of LSCF/YSZ composite electrode, on YSZ electrolyte under 250 mAcm^{-2} of cathodic current density

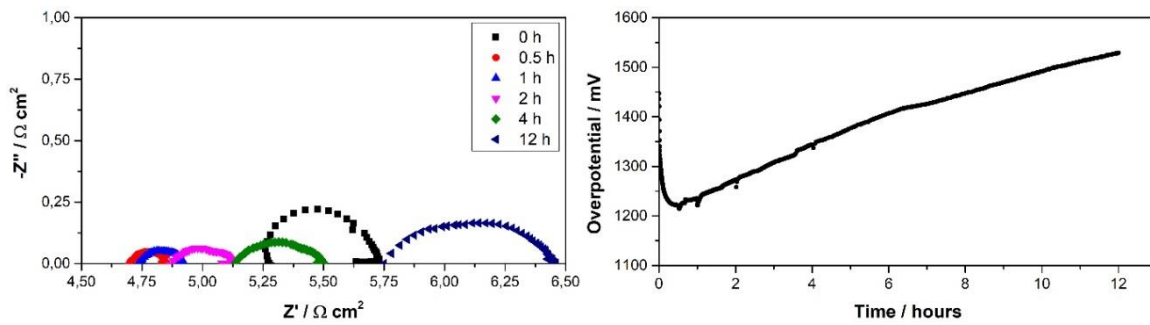


Figure 37 - Impedance and polarization curves of LSCF/YSZ composite electrode, on YSZ electrolyte under 250 mAcm^{-2} of anodic current density

Since any good results weren't obtained from LSCF/YSZ composite oxygen electrode, no further analysis was performed on this material.

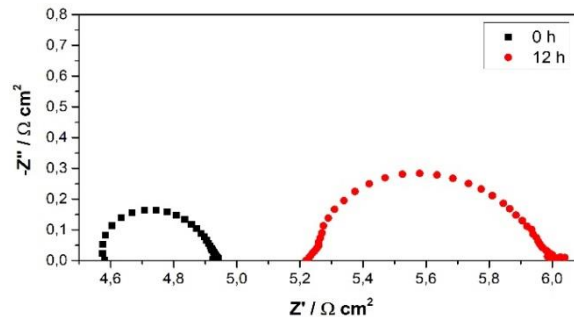


Figure 38 - Impedance and polarization curves of LSCF/YSZ composite electrode, on YSZ electrolyte before and after 12 hours of open circuit potential

Figure 38 demonstrates the bad effect that temperature has on LSCF/YSZ composite electrode. In fact, after 12 hours at $750 \text{ }^\circ\text{C}$ the polarization resistance doubled its initial value, and the electrolyte resistance increased as well.

6.2.2 LSCF/GDC

Many studies have been performed on LSCF/GDC composite electrodes, so it was not necessary to test their thermochemical compatibility.^{20, 35} The results of the cathodic polarizations, showed in Figure 39 and Figure 40, highlight very good performances. In both cases, under 250 mAcm^{-2} and 500 mAcm^{-2} of cathodic current, in both cases the overpotential keep decreasing along with the polarization resistance and the electrolyte resistance. The first test reports a very low final R_p value of only $0.05 \text{ } \Omega\text{cm}^2$ while the second one reports a higher final value of $0.19 \text{ } \Omega\text{cm}^2$.

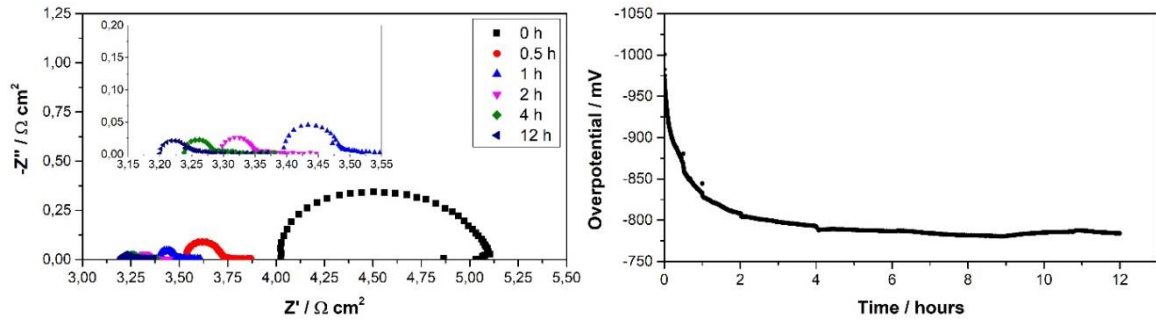


Figure 39 - Impedance and polarization curves of LSCF/GDC composite electrode, on YSZ electrolyte under 250 mAcm⁻² of cathodic current density

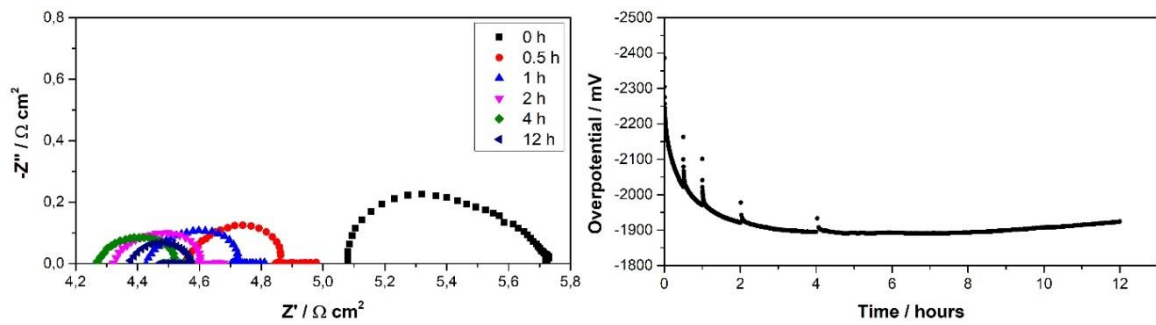


Figure 40 - Impedance and polarization curves of LSCF/GDC composite electrode, on YSZ electrolyte under 500 mAcm⁻² of cathodic current density

Figure 41 shows the SEM images of the YSZ electrolyte surface after 12 hours of cathodic polarization. The cathode was removed by adhesive tape. Very little particles are visible in the two micrographs, in the size order of 200 nm.

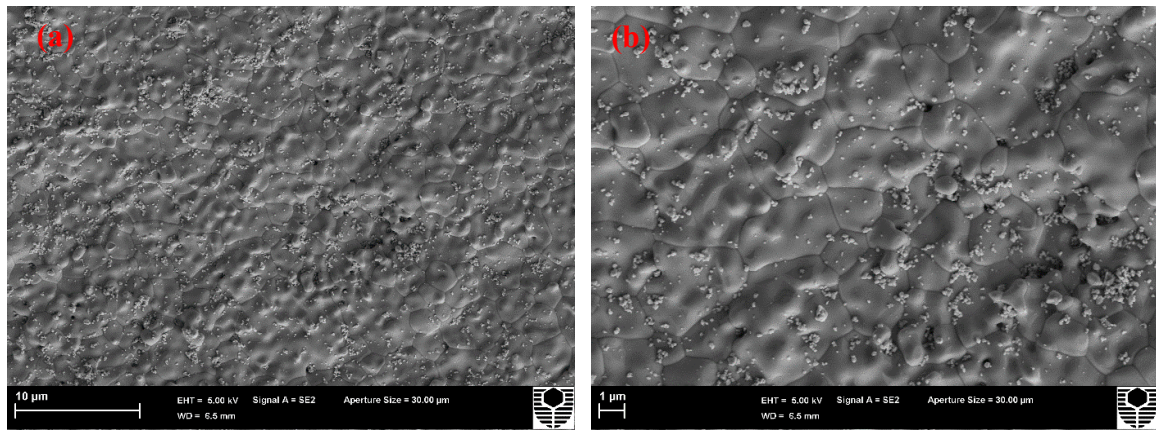


Figure 41 - SEM images of YSZ electrolyte surface after 12 hours of cathodic polarization

The electrolysis mode tests affirm very good results too. In particular, the test performed under 250 mAcm⁻² of anodic current density, reported in Figure 42, indicates a progressive overpotential reduction. This time, the overpotential reduction is not due to the polarization resistance improvement, which on the contrary continues to increase, but to the decreasing of the ohmic resistance. Despite the R_p deterioration, it shows a low initial value of 0.03 Ωcm² and a final value of 0.13 Ωcm².

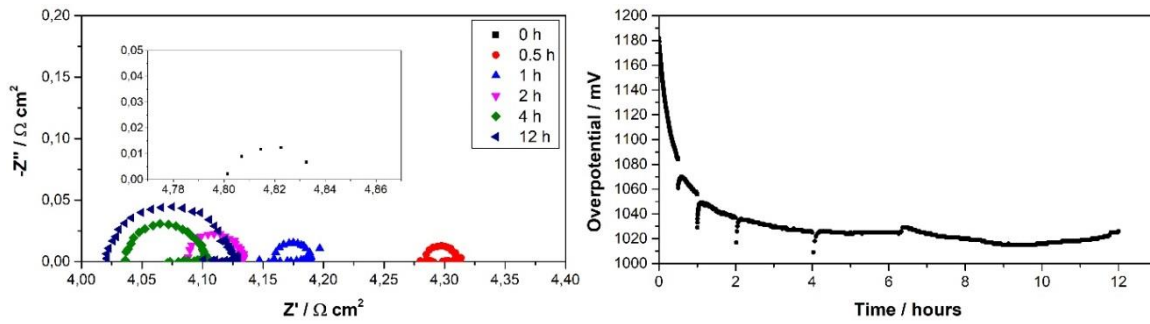


Figure 42 - Impedance and polarization curves of LSCF/GDC composite electrode, on YSZ electrolyte under 250 mAcm⁻² of anodic current density

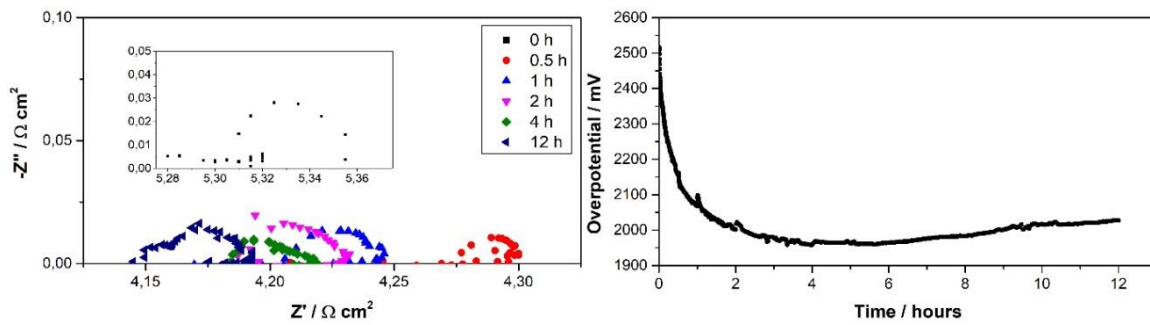


Figure 43 - Impedance and polarization curves of LSCF/GDC composite electrode, on YSZ electrolyte under 500 mAcm⁻² of anodic current density

The second test, reported in Figure 43, has a slightly different result: a constant electrolyte resistance decreasing accompanied by a quite constant polarization resistance value. In facts, all the EIS measurements performed during the test always show a value around 0.05 Ωcm².

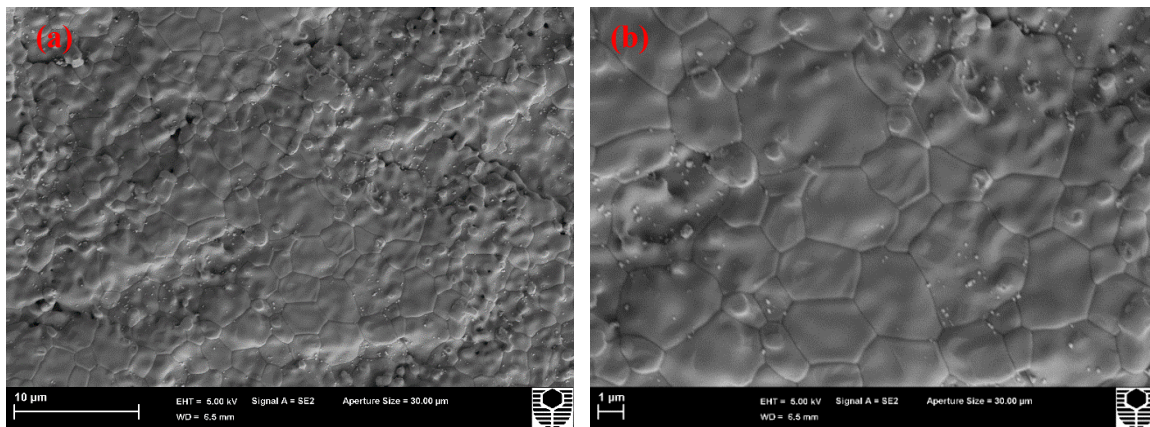


Figure 44 - SEM images of YSZ electrolyte surface after 12 hours of anodic polarization

The SEM micrographs of YSZ electrolyte surface after 12 hours of anodic polarization and after the LSCF/GDC was removed by HCl treatment are shown in Figure 44. There are some remaining particles on the YSZ surface. These particles are most likely GDC particles as they can't be dissolved in hydrochloric acid.³⁶

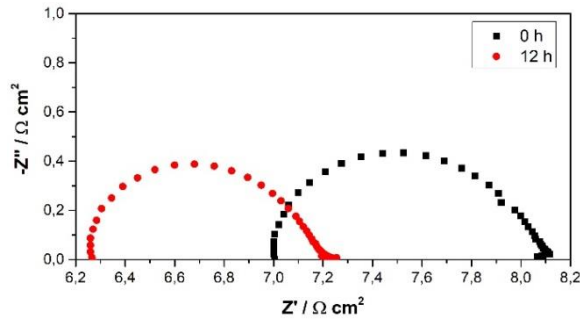


Figure 45 - Impedance and polarization curves of LSCF/GDC composite electrode, on YSZ electrolyte before and after 12 hours of open circuit potential

Nothing particularly relevant results from the 12 hours OCP test, Figure 45. As usual, the polarization resistance is not significantly affected by the temperature treatment while the ohmic resistance improves.

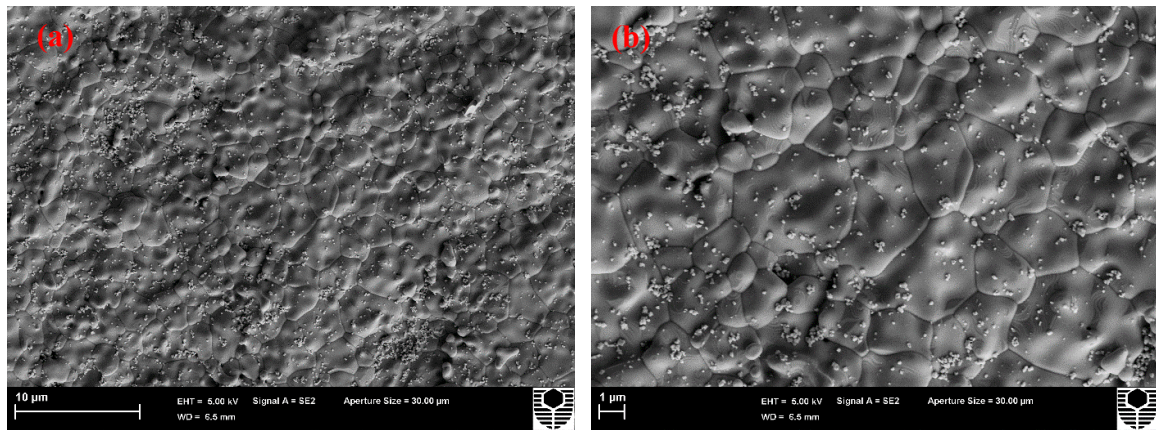


Figure 46 - SEM images of YSZ electrolyte surface after 12 hours of open circuit potential

Figure 46 shows the SEM images of the YSZ electrolyte surface after 12 hours of open circuit potential. The cathode was removed by HCl acid treatment. As for the anodic polarization case, are visible some little GDC particles, which can't be removed by acid.

6.3 BSCF

In the last years, BSCF compounds have gained increasing attention as a new cathode material for intermediate temperature SOFC applications.³⁷ As LSCF, BSCF is a mixed ions and electrons conductor. This feature makes it a perfect candidate for SOFC cathodes.

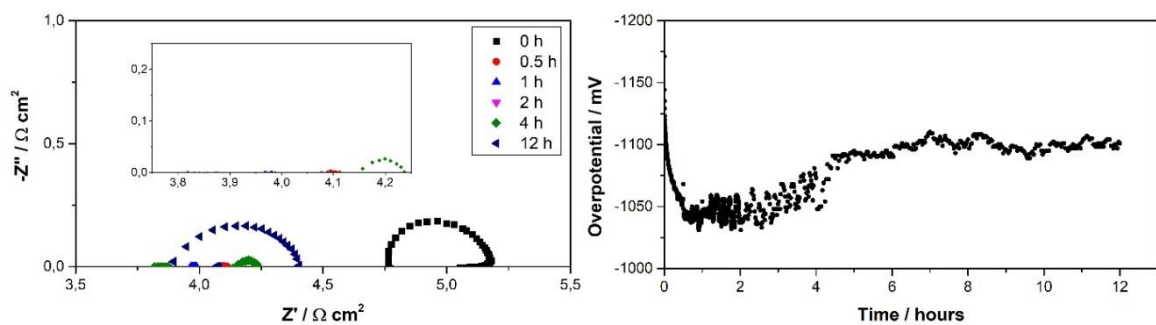


Figure 47 - Impedance and polarization curves of BSCF pristine electrode, on YSZ electrolyte under 250 mAcm^{-2} of cathodic current density

However, the use of pristine BSCF cathode is not suggested. Figure 47 shows the results of a cathodic polarization performed under 250 mAcm^{-2} of current density. Despite some very small polarization resistance values measured with EIS analysis, so small that they are not even easily quantifiable, the overpotential trend is very irregular, and at the very last the performance of the half-cell deteriorates quickly, suggesting a chemical instability.

6.3.1 BSCF/YSZ

First of all, a thermochemical compatibility test was performed in order to understand if there are some problems related to the use of YSZ and BSCF together at high temperatures. The result of the test, shown in Figure 48, confirms that there aren't compatibility issues at temperatures as high as $800 \text{ }^\circ\text{C}$.

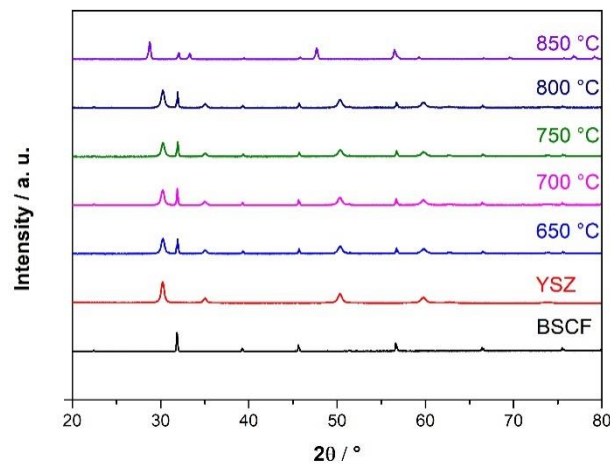


Figure 48 - XRD thermochemical compatibility test between BSCF and YSZ

The results of the two tests performed under cathodic polarization, respectively at 250 mAcm^{-2} and 500 mAcm^{-2} of current density, are almost identical. During the first test, Figure 49, the reduction of the overpotential is caused by the continuous improvement of the half-cell performances. Both the electrolyte resistance and the polarization resistance reduce their values. The former goes from $8.3 \text{ } \Omega\text{cm}^2$ to $5.3 \text{ } \Omega\text{cm}^2$ and the latter goes from $1.0 \text{ } \Omega\text{cm}^2$ to $0.5 \text{ } \Omega\text{cm}^2$. Similarly, during the second test, Figure 50, the overpotential decreases according to the improvement of the two resistances. R_p goes from $1.1 \text{ } \Omega\text{cm}^2$ to $0.3 \text{ } \Omega\text{cm}^2$ and R_Ω goes from $9.2 \text{ } \Omega\text{cm}^2$ to $5.3 \text{ } \Omega\text{cm}^2$.

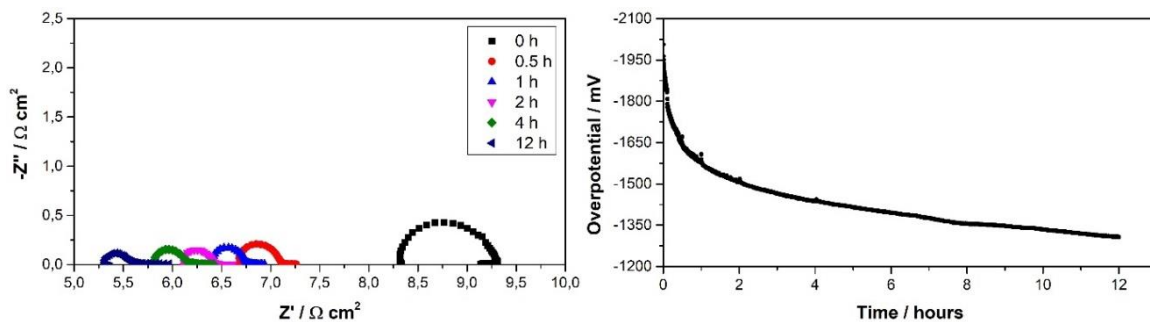


Figure 49 - Impedance and polarization curves of BSCF/YSZ composite electrode, on YSZ electrolyte under 250 mAcm^{-2} of cathodic current density

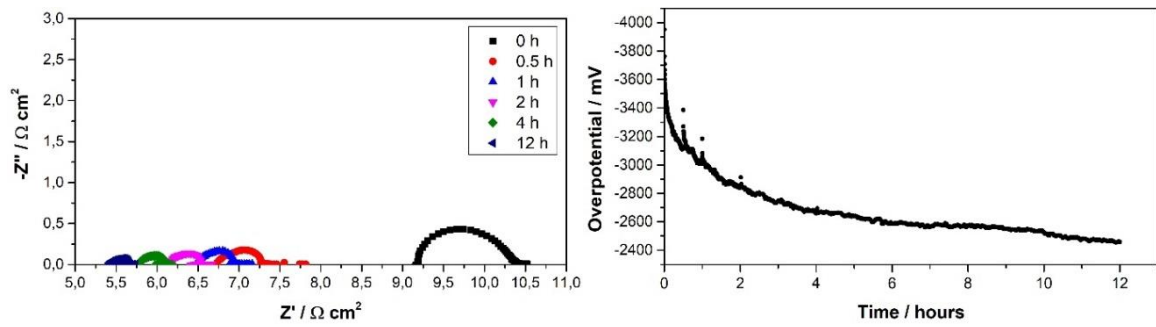


Figure 50 - Impedance and polarization curves of BSCF/YSZ composite electrode, on YSZ electrolyte under 500 mAcm^{-2} of cathodic current density

Figure 51 shows two SEM micrographs at different magnification of the YSZ electrolyte surface after 12 hours of cathodic polarization. The cathode layer was removed by adhesive tape.

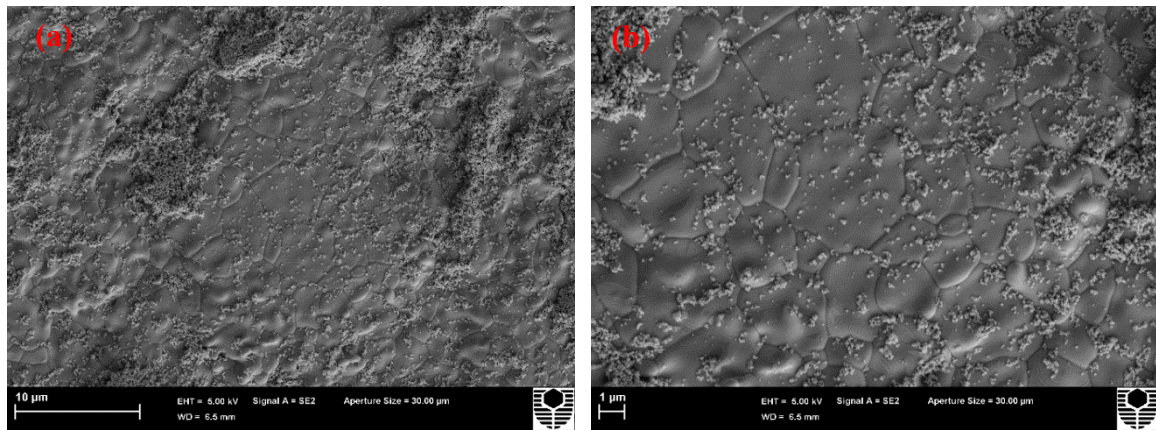


Figure 51 - SEM images of YSZ electrolyte surface after 12 hours of cathodic polarization

The tests performed under anodic polarization reflect the results obtained by the tests performed under cathodic polarization. Figure 52 shows the outcome of the test carried out under 250 mAcm^{-2} of anodic current density. The main cause of the overpotential improvement is the ohmic resistance drop: it starts the test at 7.7 Ωcm^2 and ends it at 5.1 Ωcm^2 . The decrease in the polarization resistance is not so significant: after a low initial reduction, its value settles down around 0.5 Ωcm^2 .

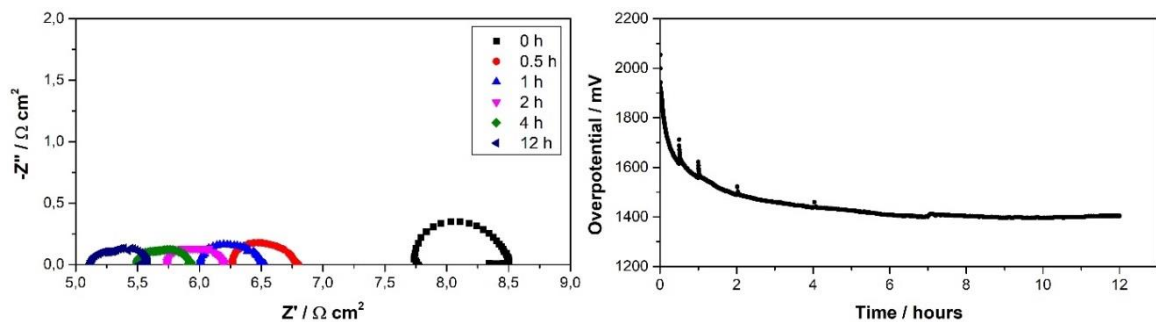


Figure 52 - Impedance and polarization curves of BSCF/YSZ composite electrode, on YSZ electrolyte under 250 mAcm^{-2} of anodic current density

The second anodic test, reported in Figure 53, shows a different situation. In this second case, both the ohmic resistance and the polarization resistant improve significantly. The

former keeps decreasing until the end with a final value of $5.2 \Omega\text{cm}^2$, the latter reaches a noteworthy final value of $0.06 \Omega\text{cm}^2$, but during the test, it reached even lower values.

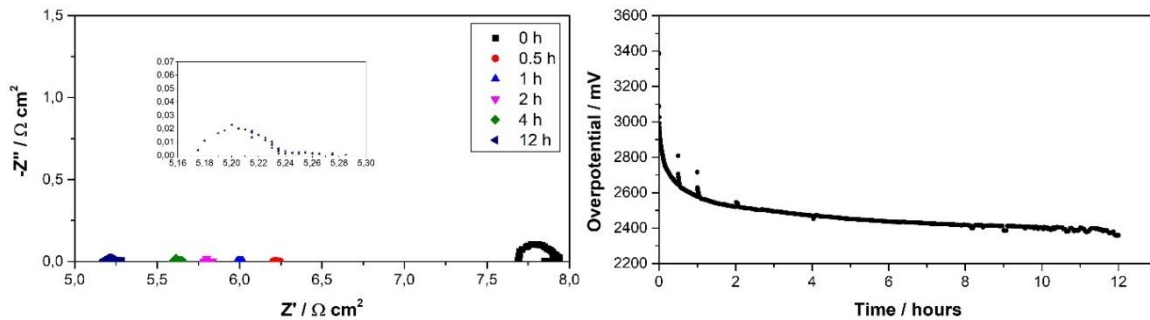


Figure 53 - Impedance and polarization curves of BSCF/YSZ composite electrode, on YSZ electrolyte under 500 mAcm^{-2} of anodic current density

The SEM images reported in Figure 54 show the YSZ electrolyte surface after 12 hours of anodic polarization. The removal of the composite electrode layer was performed via adhesive tape. The circle in Figure 54a highlights some residual particles of the BSCF perovskite structure.

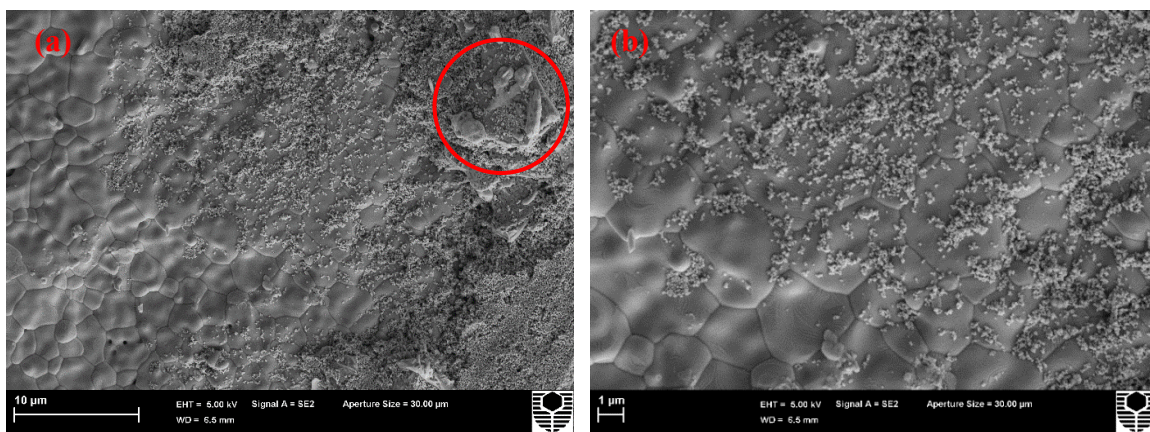


Figure 54 - SEM images of YSZ electrolyte surface after 12 hours of anodic polarization

The outcome of the 12 hours OCP test, shown in Figure 55, confirms that temperature doesn't affect the polarization resistance, but only increases the contact points between electrode and electrolyte, reducing the ohmic resistance.

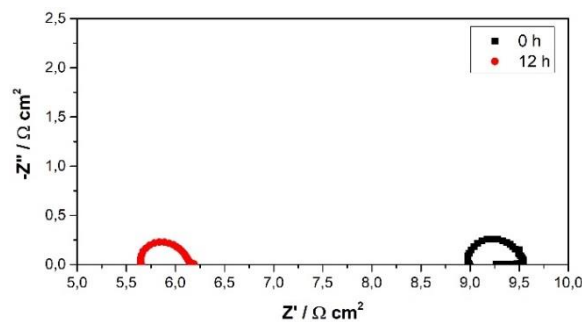


Figure 55 - Impedance and polarization curves of BSCF/YSZ composite electrode, on YSZ electrolyte before and after 12 hours of open circuit potential

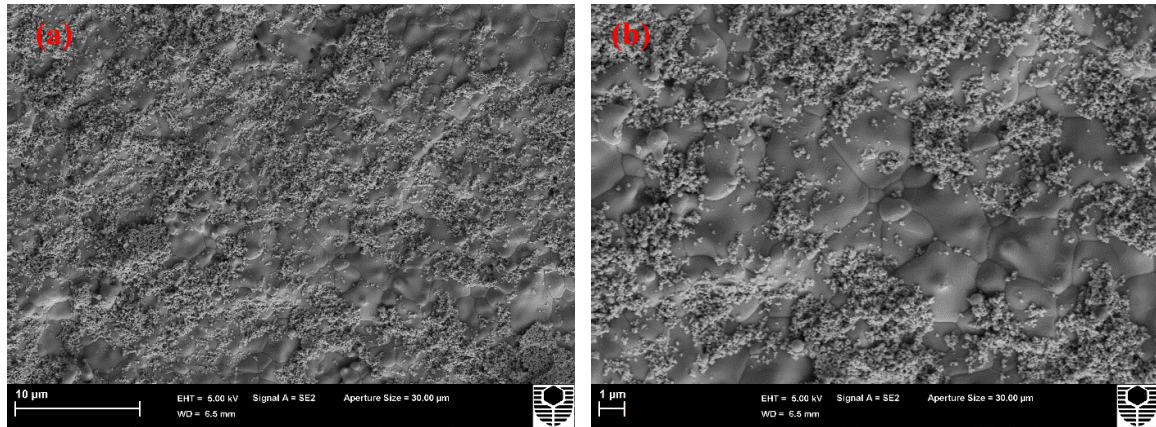


Figure 56 - SEM images of YSZ electrolyte surface after 12 hours of open circuit potential

In Figure 56 are shown the SEM images of the YSZ electrolyte surface after 12 hours of open circuit potential. The electrode was peeled off using adhesive tape. As usual, only small particles are visible on YSZ electrolyte surface.

6.3.2 BSCF/GDC

As already done with BSCF/YSZ composite oxygen electrode, an XRD thermochemical compatibility test was performed between BSCF and GDC. Figure 57 shows the outcome of the test and confirms that BSCF and GDC are chemically compatible at temperature as high as 850 °C, and maybe higher.

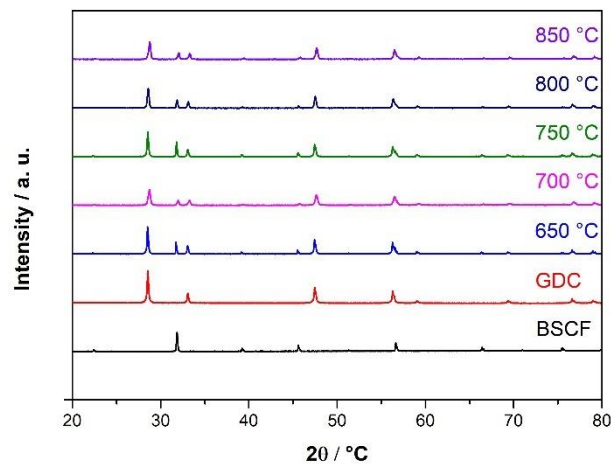


Figure 57 - XRD thermochemical compatibility test between BSCF and GDC

Figure 58 and Figure 59 report the results of the two electrochemical tests performed on BSCF/GDC under cathodic polarization, respectively at 250 mAcm⁻² and 500 mAcm⁻² of current density. The first test shows a continuous decrease of the overpotential, partially due to the reduction of the ohmic resistance (from 5.5 Ωcm² to 4.5 Ωcm²) and partially due to the reduction of the polarization resistance (from 0.80 Ωcm² to lower than 0.01 Ωcm²). The result of this test is particularly interesting because among all the test performed, it is the one that shows the better cathodic performance. The second cathodic test performed on BSCF/GDC points out good performances too. The ohmic resistance drops from 9.1 Ωcm² to 6.4 Ωcm² and the polarization resistance from 0.9 Ωcm² to a good final value of 0.2 Ωcm².

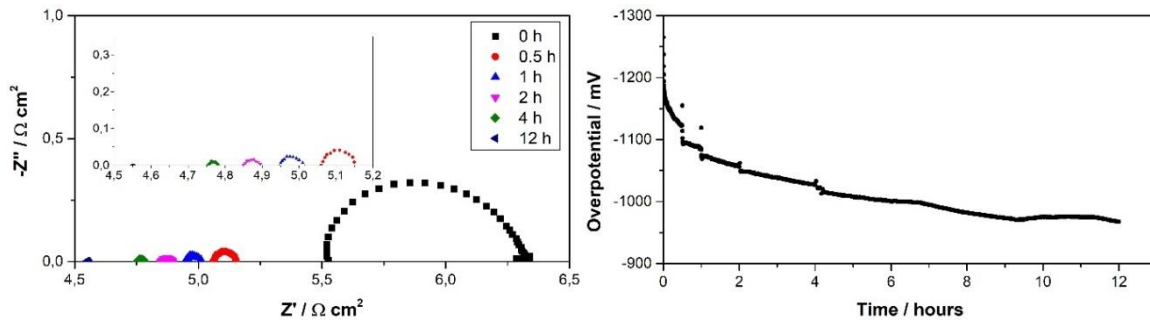


Figure 58 - Impedance and polarization curves of BSCF/GDC composite electrode, on YSZ electrolyte under 250 mAcm⁻² of cathodic current density

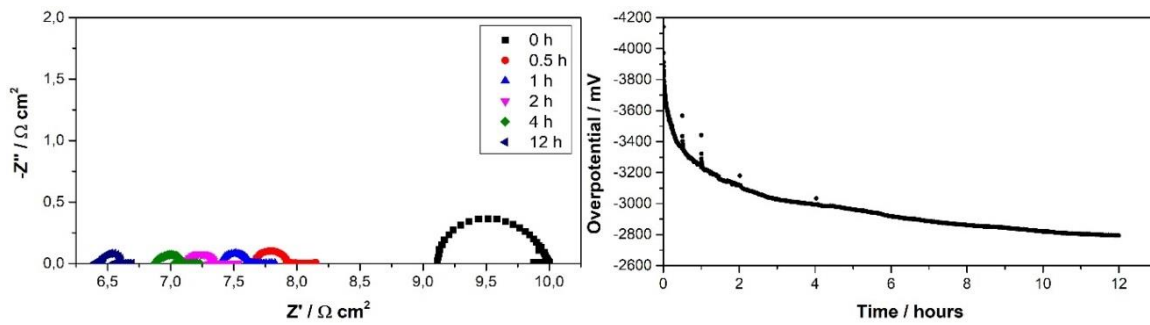


Figure 59 - Impedance and polarization curves of BSCF/GDC composite electrode, on YSZ electrolyte under 500 mAcm⁻² of cathodic current density

Figure 60 shows the SEM images of the YSZ electrolyte surface after 12 hours of cathodic polarization at different magnifications. The cathode coating was removed by adhesive tape. In the images is possible to see small GDC particles, difficult to remove, and some bigger BSCF particles highlighted in Figure 60b.

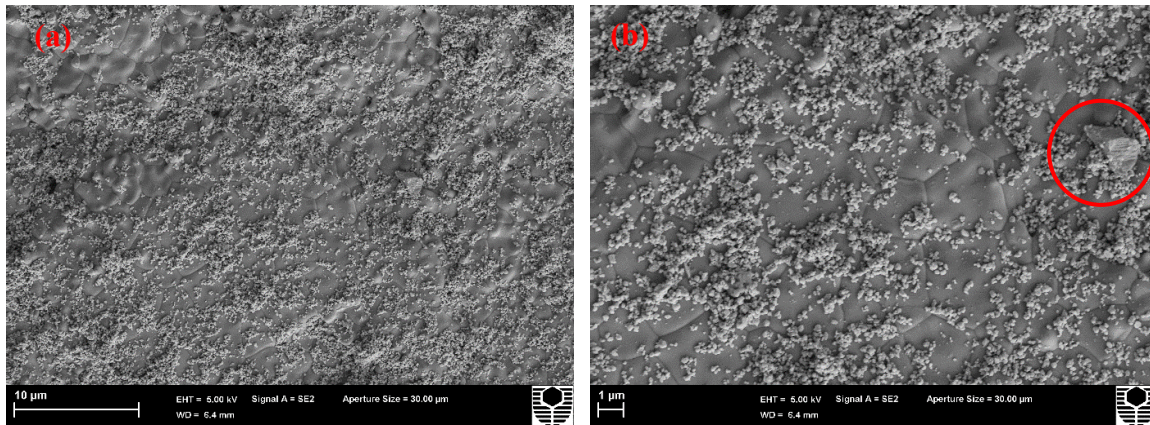


Figure 60 - SEM images of YSZ electrolyte surface after 12 hours of cathodic polarization

A similar situation is presented by the anodic electrochemical tests. The 250 mAcm⁻² current density test shows a very good and stable overpotential decreasing trend, Figure 61. The polarization resistance decreases from 1.3 Ωcm² to 0.2 Ωcm² and the ohmic resistance drops from 9.7 Ωcm² to 7.2 Ωcm². In Figure 62, the outcome of the second anodic test is reported. Despite the good values of the polarization values and the excellent ohmic resistance, the overpotential trend is very unstable.

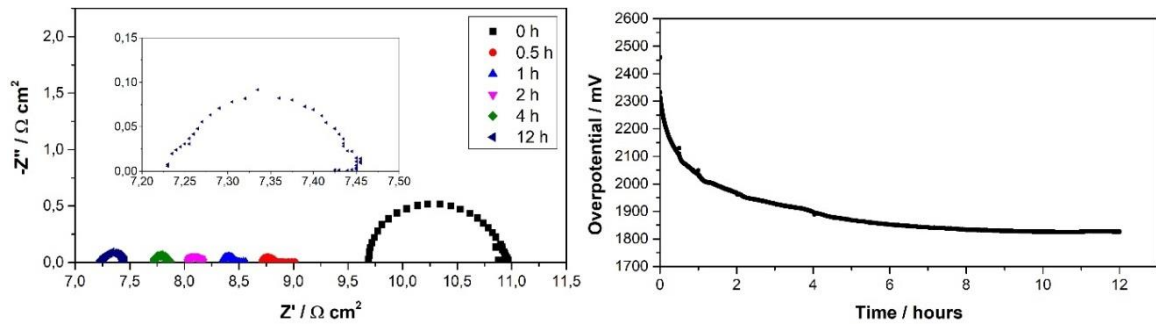


Figure 61 - Impedance and polarization curves of BSCF/GDC composite electrode, on YSZ electrolyte under 250 mAcm⁻² of anodic current density

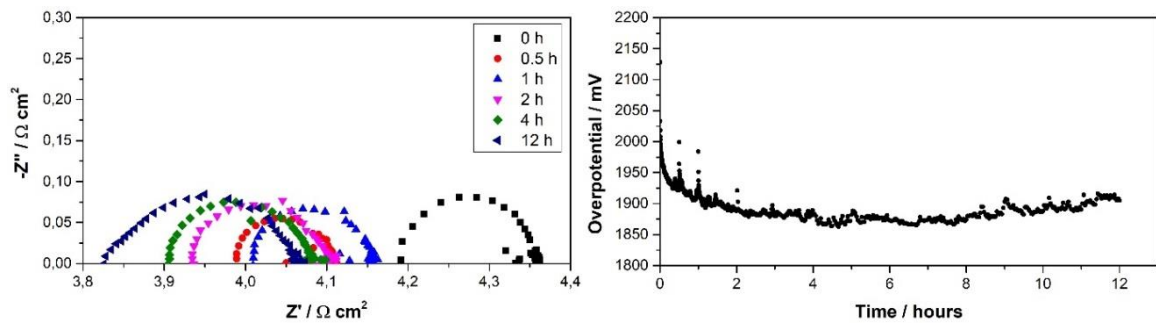


Figure 62 - Impedance and polarization curves of BSCF/GDC composite electrode, on YSZ electrolyte under 500 mAcm⁻² of anodic current density

The SEM images reported in Figure 63 show the YSZ electrolyte surface after 12 hours of anodic polarization. The removal of the composite electrode layer was performed via adhesive tape.

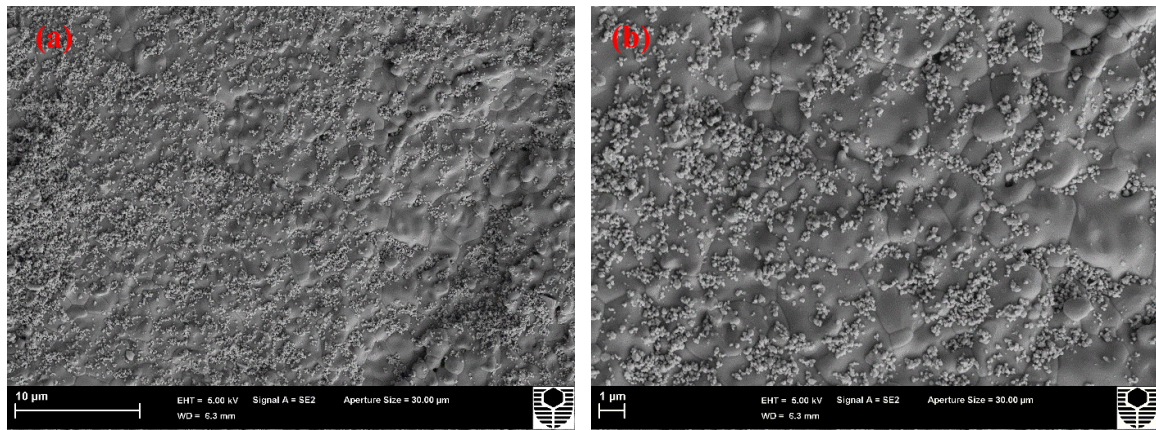


Figure 63 - SEM images of YSZ electrolyte surface after 12 hours of anodic polarization

The final test performed on BSCF/GDC composite oxygen electrode is the 12 hours OCP test. The outcome of the test confirms that the 750 °C temperature treatment doesn't affect the polarization resistance. The temperature helps decreasing the ohmic resistance, that goes from 7.0 Ωcm² to 5.3 Ωcm². The result of the test is shown in Figure 64.

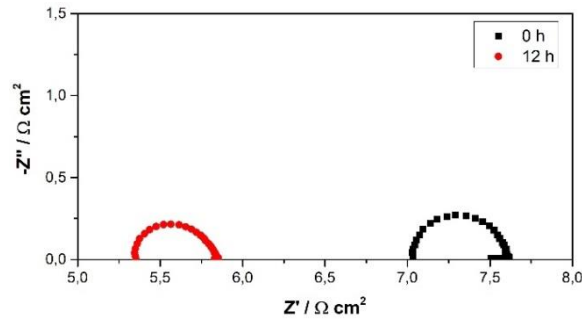


Figure 64 - Impedance and polarization curves of BSCF/GDC composite electrode, on YSZ electrolyte before and after 12 hours of open circuit potential

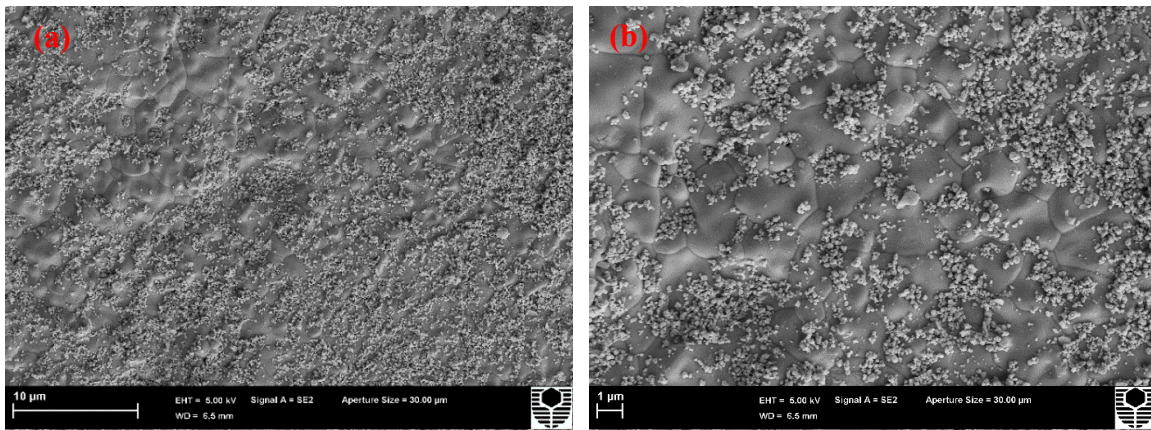


Figure 65 - SEM images of YSZ electrolyte surface after 12 hours of open circuit potential

Figure 65 shows the SEM images of the YSZ electrolyte surface after 12 hours of open circuit potential. The composite electrode was removed using adhesive tape. As for the previous test, only some small particles are visible.

6.4 NBCaC

NBCaC is a novel SOFC cathode material, intensively studied in the last few years. Some studies report excellent performances of this material at temperatures lower than 700 °C.¹⁵

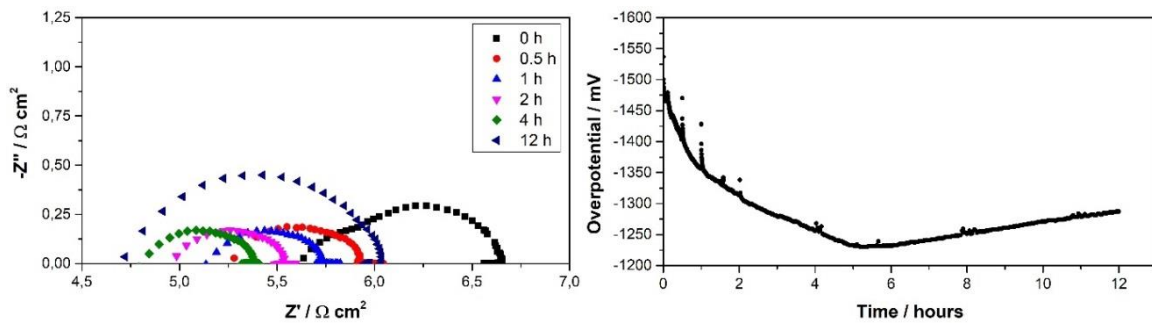


Figure 66 - Impedance and polarization curves of NBCaC pristine electrode, on YSZ electrolyte under 250 mAcm⁻² of cathodic current density

Figure 66 shows the cathodic test performed on NBCaC pristine electrode. For the first 5 hours, the overpotential trend is strongly decreasing, according to a progressive ohmic resistance reduction. Then, all of a sudden, the trend is reversed, and the polarization resistance more than double its value.

6.4.1 NBCaC/YSZ

First of all, in order to test the thermochemical compatibility of NBCaC and YSZ, an XRD compatibility test was performed.

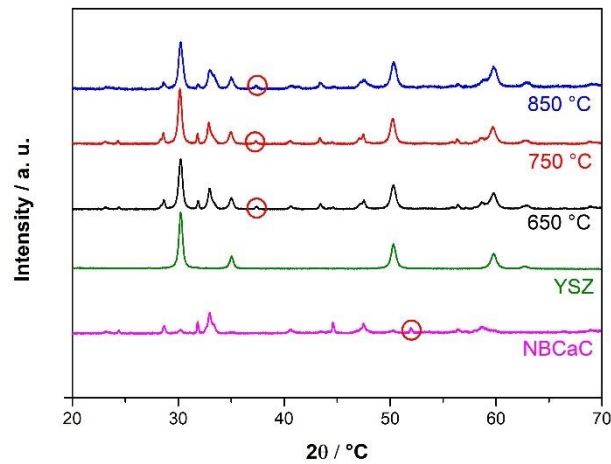


Figure 67 - XRD thermochemical compatibility test between NBCaC and YSZ

The result of the test, shown in Figure 67, highlights the formation of a small peak and the elimination of another one. This could probably mean that the temperature could help the formation of a new phase between NBCaC and YSZ.

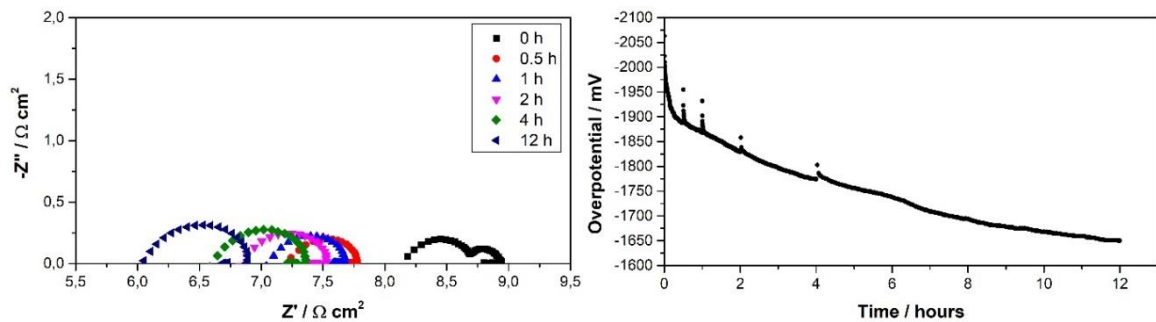


Figure 68 - Impedance and polarization curves of NBCaC/YSZ composite electrode, on YSZ electrolyte under 250 mAcm^{-2} of cathodic current density

Figure 68 shows the results of the first cathodic test, performed under 250 mAcm^{-2} of current density. Despite a good reduction of the overpotential, driven by the ohmic resistance improvement, the polarization continues to increase, with a final value of 0.9 Ωcm^2 .

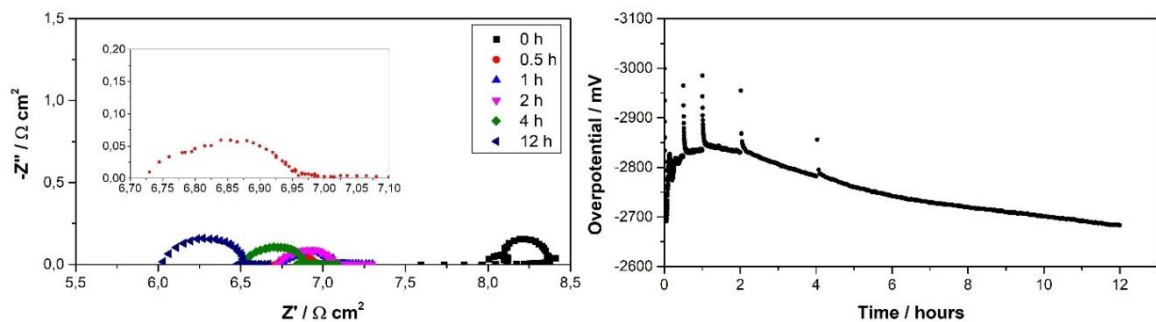


Figure 69 - Impedance and polarization curves of NBCaC/YSZ composite electrode, on YSZ electrolyte under 500 mAcm^{-2} of cathodic current density

The same situation is confirmed by the second cathodic test. The result, reported in Figure 69, shows a quick polarization resistance reduction, followed by a progressive increase, with a final value of $0.5 \Omega\text{cm}^2$.

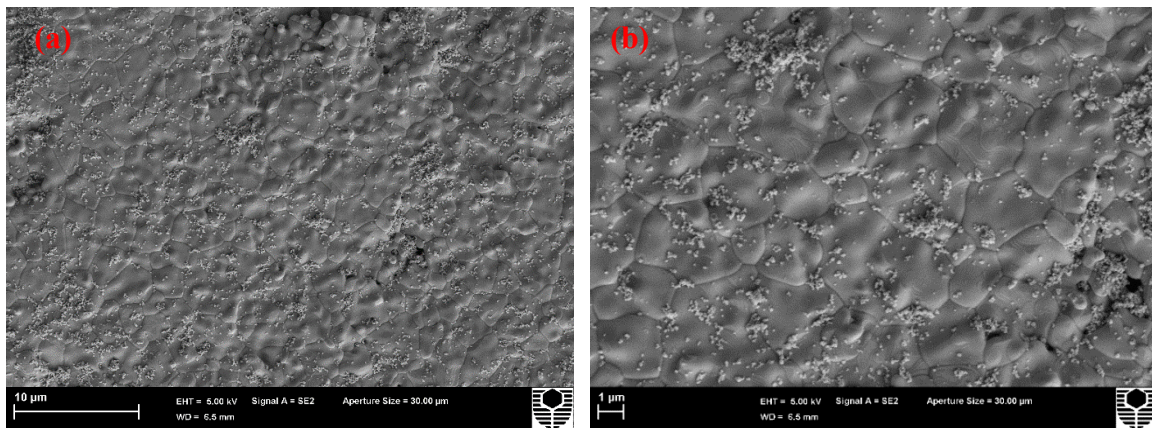


Figure 70 - SEM images of YSZ electrolyte surface after 12 hours of cathodic polarization

Figure 70 shows the YSZ surface in contact with the oxygen electrode after the cathodic polarization. The cathode layer was removed via adhesive tape. It is still possible to see some small particles attached to the electrolyte surface.

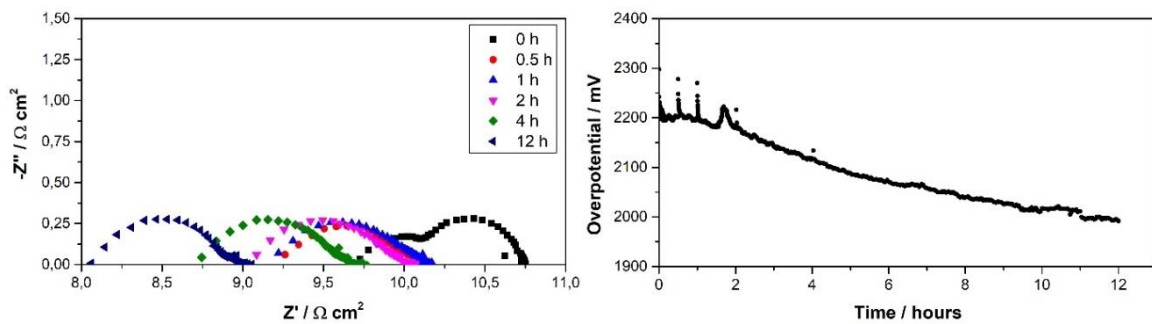


Figure 71 - Impedance and polarization curves of NBCaC/YSZ composite electrode, on YSZ electrolyte under 250 mAcm^{-2} of anodic current density

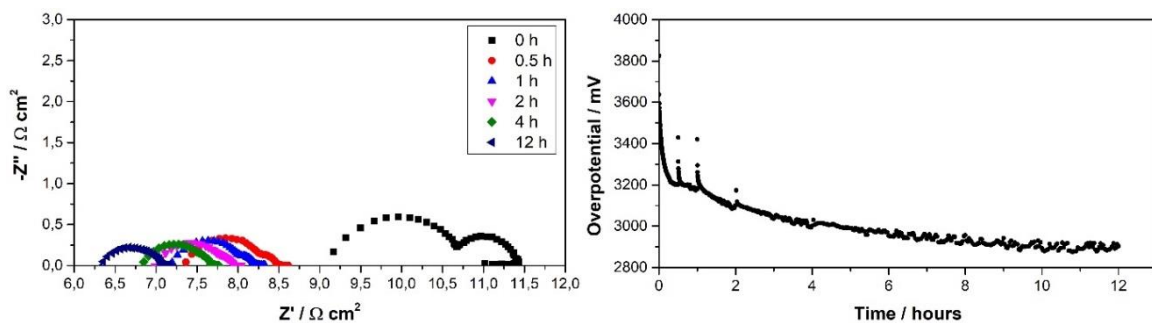


Figure 72 - Impedance and polarization curves of NBCaC/YSZ composite electrode, on YSZ electrolyte under 500 mAcm^{-2} of anodic current density

The anodic tests performed on NBCaC/YSZ composite electrode have a different outcome. The test performed under 250 mAcm^{-2} of anodic current density, shown in Figure 71, report a continuous ohmic resistance decrease while the polarization resistance is constant at $0.9 \Omega\text{cm}^2$. Figure 72 shows a better result: both the ohmic and the

polarization resistances keep decreasing with final values respectively of $6.3 \Omega\text{cm}^2$ and $0.7 \Omega\text{cm}^2$.

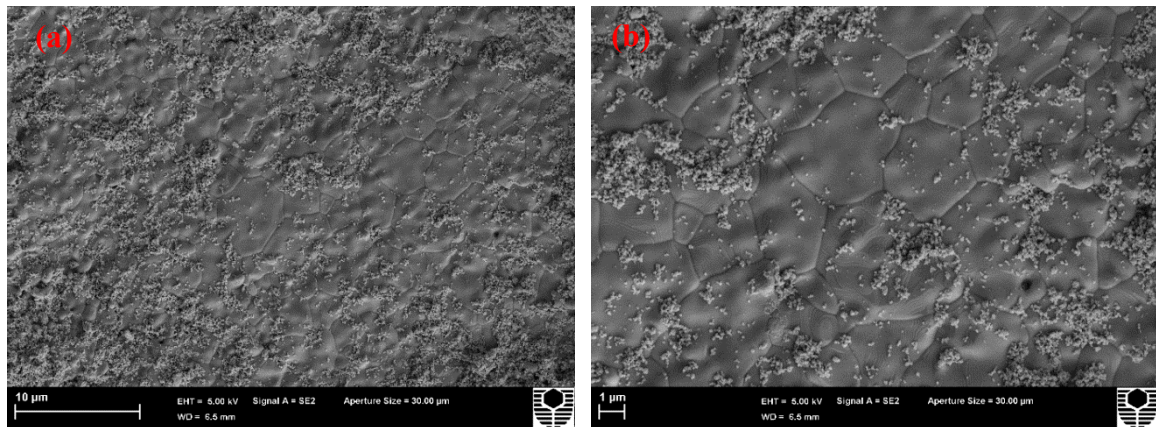


Figure 73 - SEM images of YSZ electrolyte surface after 12 hours of anodic polarization

Figure 73 shows two SEM micrographs at two different magnifications of the YSZ electrolyte surface after the anodic polarization. On the surface, after the electrode removal via adhesive tape, it is still possible to see some electrode's residual particles.

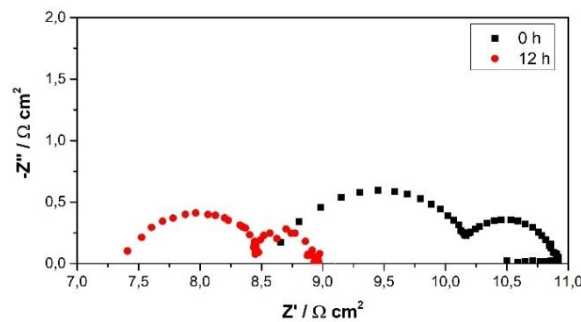


Figure 74 - Impedance and polarization curves of NBCaC/YSZ composite electrode, on YSZ electrolyte before and after 12 hours of open circuit potential

Surprisingly, Figure 74 seems to assert that the temperature helps to improve both the ohmic and the polarization resistances. In fact, both of them decrease during the 12 hours OCP test.

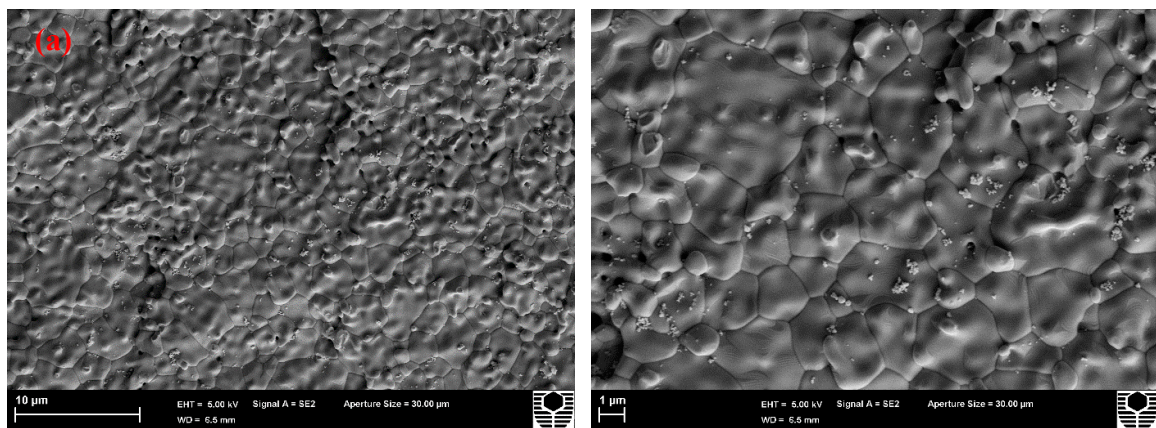


Figure 75 - SEM images of YSZ electrolyte surface after 12 hours of open circuit potential

In Figure 75, are reported the SEM images of the YSZ electrolyte surface after 12 hours of open circuit potential. The cathode layer was removed by hydrochloric acid. Therefore, the surface appears to be very clean.

6.4.2 NBCaC/GDC

Compared to NBCaC/YSZ, NBCaC/GDC composite electrode has been studied by much more researchers. This is the reason why it was not necessary to perform a thermochemical compatibility test.²⁹

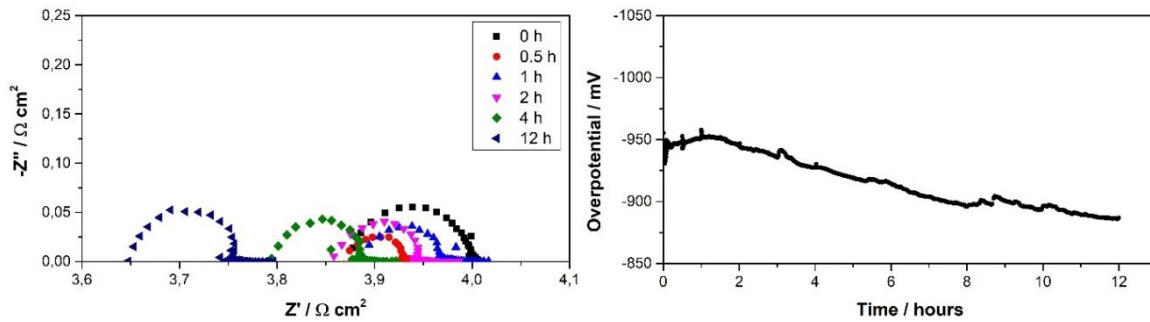


Figure 76 - Impedance and polarization curves of NBCaC/GDC composite electrode, on YSZ electrolyte under 250 mAcm⁻² of cathodic current density

The two electrochemical tests performed under cathodic polarization, give two different outcomes. The first one, reported in Figure 76, shows a very low overpotential, thanks to low values of polarization and ohmic resistances, with final values of respectively 0.10 Ωcm² and 3.65 Ωcm².

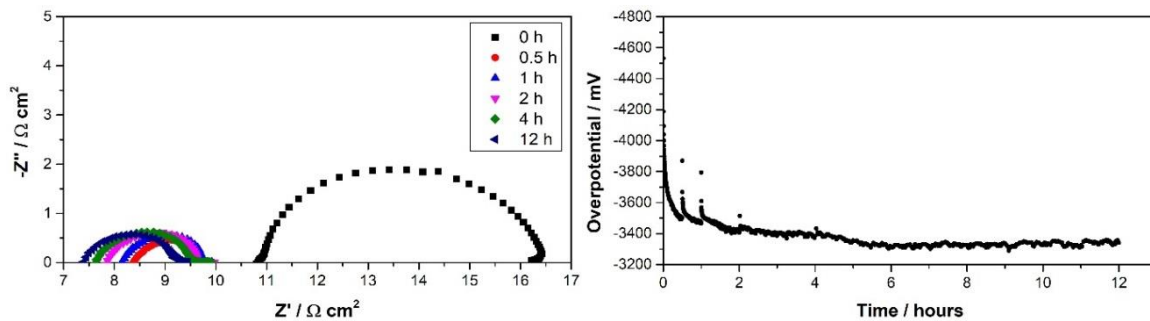


Figure 77 - Impedance and polarization curves of NBCaC/GDC composite electrode, on YSZ electrolyte under 500 mAcm⁻² of cathodic current density

The results of the second test, performed under 500 mAcm⁻² of cathodic current density, are shown in Figure 77. The first EIS measurement reports 11 Ωcm² of ohmic resistance and a really high polarization resistance, higher than 5 Ωcm². After the first half an hour, the polarization resistance drops and settles down around 1.5 Ωcm². Meanwhile, the ohmic resistance drops too, with a final value of 7.5 Ωcm². This high resistances values turn into an extremely high overpotential.

Figure 78 shows the SEM micrographs of the YSZ electrolyte surface after the 12 hours of cathodic polarization. The composite cathode layer was peeled off using adhesive tape. Attached to the electrolyte surface, it is possible to see small composite cathode residual particles.

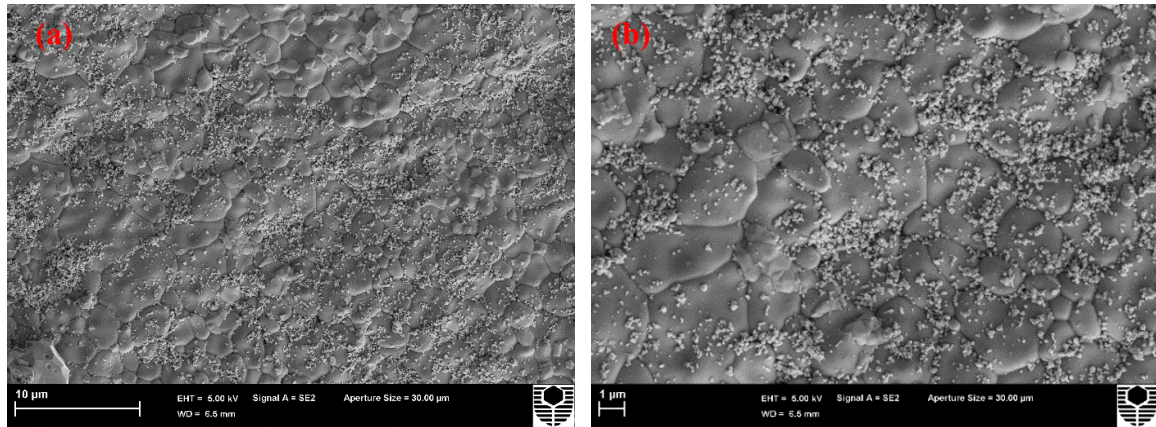


Figure 78 - SEM images of YSZ electrolyte surface after 12 hours of cathodic polarization

Figure 79 and Figure 80 show the results of the anodic polarization tests. The first one, performed under 250 mAcm^{-2} of current density, shows very low polarization resistance. The final value is about $0.04 \text{ } \Omega\text{cm}^2$. The ohmic resistance drops from $10.6 \text{ } \Omega\text{cm}^2$ to $4.8 \text{ } \Omega\text{cm}^2$.

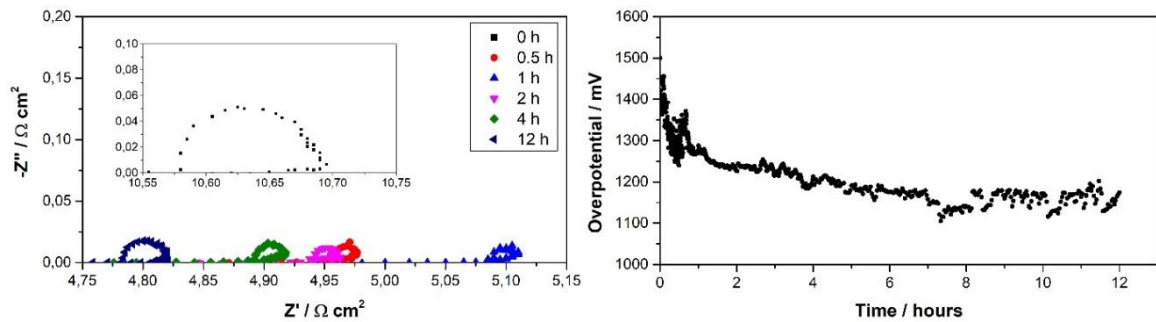


Figure 79 - Impedance and polarization curves of NBCaC/GDC composite electrode, on YSZ electrolyte under 250 mAcm^{-2} of anodic current density

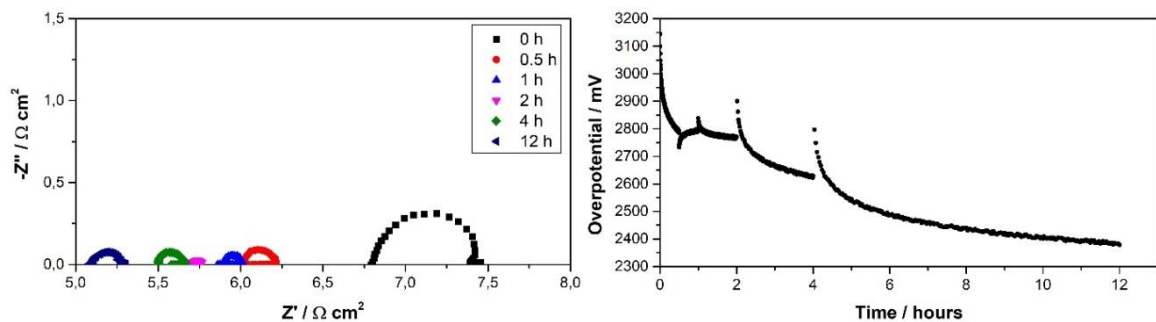


Figure 80 - Impedance and polarization curves of NBCaC/GDC composite electrode, on YSZ electrolyte under 500 mAcm^{-2} of anodic current density

The 500 mAcm^{-2} anodic current density test shows a constant overpotential decrease, due to the ohmic and the polarization resistances improvement. The final value of the polarization resistance is around $0.2 \text{ } \Omega\text{cm}^2$, but during the test, it reached even lower values.

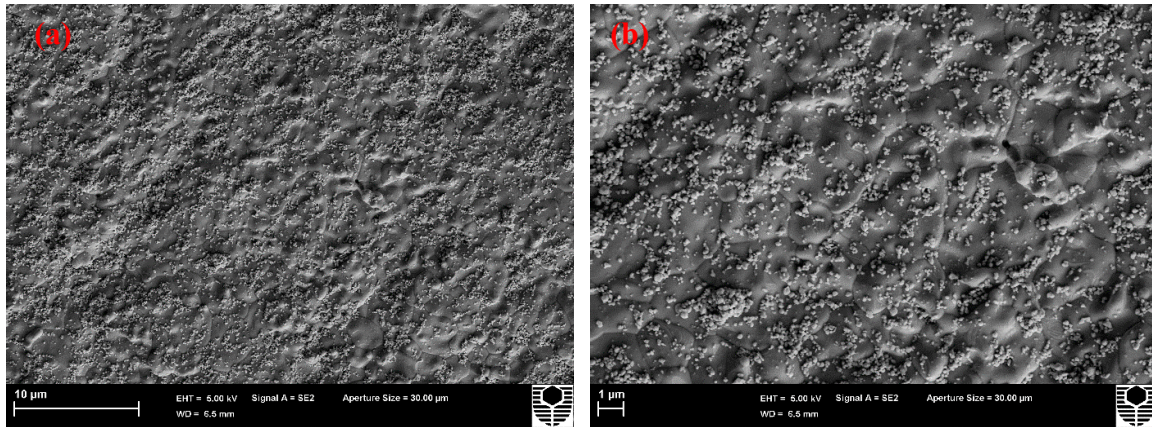


Figure 81 - SEM images of YSZ electrolyte surface after 12 hours of anodic polarization

Figure 81 shows two SEM micrographs at two different magnifications of the YSZ electrolyte surface after the anodic polarization. The electrode layer was removed via adhesive tape.

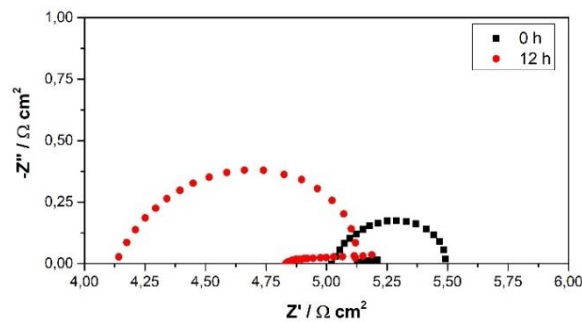


Figure 82 - Impedance and polarization curves of NBCaC/GDC composite electrode, on YSZ electrolyte before and after 12 hours of open circuit potential

The last test performed on NBCaC/GDC composite electrode is the 12 hours OCP test. The result of the test, shown in Figure 82, confirms that the temperature treatment doesn't affect positively the polarization resistance of the cell. On the contrary, it increases its value.

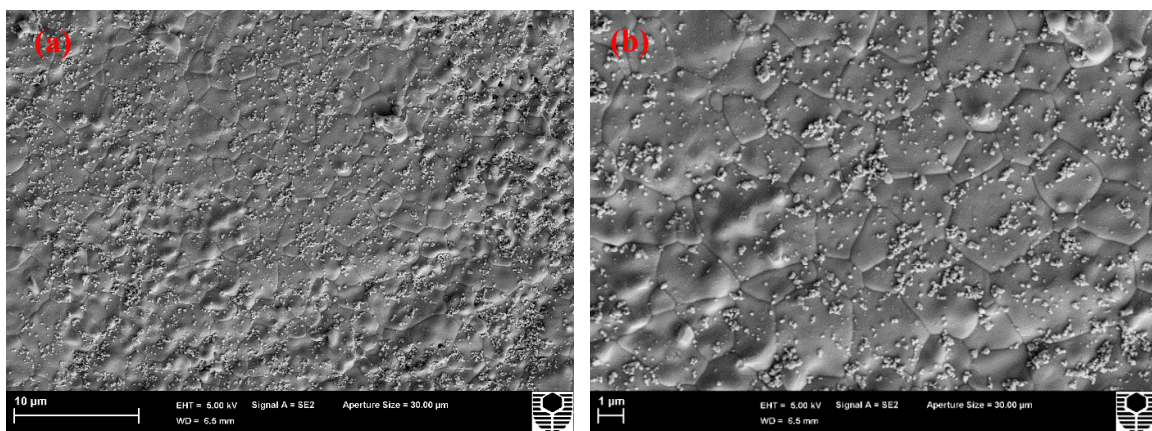


Figure 83 - SEM images of YSZ electrolyte surface after 12 hours of open circuit potential

In Figure 83 are shown the SEM images of the YSZ electrolyte surface after 12 hours of open circuit potential. The cathode was removed by adhesive tape.

7 Conclusions

In this study, the use of directly assembled composite oxygen electrode on barrier-layer-free YSZ electrolyte of SOECs was investigated in detail. The elimination of high temperature sintering steps and the simplicity of the in-situ approach enable the incorporation of highly active but chemically and thermally stable materials, to substantially enhance the electrocatalytic activity and stability of solid oxide fuel cells. The most relevant outcomes of the current study are listed below.

- The in-situ approach is a good method for the fabrication of SOFC. The polarization allows to form a good electrolyte/electrode interface, showing that high temperature sintering processes are not fundamental for the formation of a solid/solid interface.
- In general, the results show better performances of the GDC based composite electrodes. The use of GDC is preferred rather than YSZ in the fabrication of composite oxygen electrodes for low to intermediate temperature solid oxide fuel cells. As a matter of fact, the oxygen ions conductivity of GDC is higher than the one of YSZ, even at reduced temperature. Furthermore, unlike YSZ, GDC has not thermochemical compatibility problems with cobaltite-based perovskite electrodes, such as LSCF, BSCF or NBCaC.
- LSM based electrodes are well known to be chemically and thermally stable, but its properties rapidly deteriorate at temperatures lower than 800 °C. Thus, it is not a good candidate for low to intermediate temperature SOFCs.
- LSCF is a good mixed ions and electrons conductor, and this characteristic is a fundamental requirement for having acceptable performances in a low temperature range. However, LSCF suffers from strontium segregation.³⁸ Therefore, LSCF requires to be mixed with some stabilizing phase, to be doped or to be periodically polarized under anodic conditions in order to prevent (or recover) the strontium segregation.³⁹ Finally, LSCF is well known to be highly reactive with YSZ, so a certain amount of caution is required when using these two materials together.
- BSCF is a more recent MIEC used as a cathode for solid oxide fuel cells. It showed excellent performances both under cathodic and anodic polarization, especially when mixed with GDC ions conductor.
- NBCaC is one of the most recently studied materials used for SOFC cathodes. Its particular double perovskite structure should further improve its properties, such as the ionic and electronic conductivities. Although it is possible to find some excellent results reported in literature about the use of this material in SOFC, the results achieved by this study are good but sometimes discordant. More efforts should be spent on the study of this material.

This is to be intend as a preliminary study. The in-situ approach has been used for the fabrication of several electrolytes supported solid oxide half cells. Four different materials (LSM, LSCF, BSCF and NBCaC) have been mixed with two oxygen ions conductor (YSZ and GDC) obtaining eight composite oxygen electrodes. Every composite oxygen electrode has been tested under cathodic polarization, anodic polarization and OCP using 12 hours electrochemical tests at 750 °C. Then, the results of the tests have been studied and commented. In order to complete this study, it would be necessary to carry on some stability tests, that is to perform the electrochemical tests for a period longer than 12 hours, at least 100 hours. In this way it would be possible to study the durability of the

composite electrodes. Another important aspect would be to study the behaviour of the electrodes in a CO₂ rich atmosphere. The final step would be to test the most promising composite electrodes on an anode supported full cell, in order to evaluate the performances of the complete solid oxide cells.

8 Bibliography

1. Jiang SP. Thermally and Electrochemically Induced Electrode/Electrolyte Interfaces in Solid Oxide Fuel Cells: An AFM and EIS Study. *J Electrochem Soc.* 2015;162(10):F1119-F1128. doi:10.1149/2.0111510jes
2. Fergus J, Hui R, Li X, Wilkinson DP, Zhang J. *Solid Oxide Fuel Cells: Materials Properties and Performance*. CRC Press; 2016. <https://books.google.com.au/books?id=TM0-YRvUbioC>.
3. Jiang SP. *Development of Lanthanum Strontium Manganite Perovskite Cathode Materials of Solid Oxide Fuel Cells: A Review*. Vol 43.; 2008. doi:10.1007/s10853-008-2966-6
4. Bockris OM, Reddy AKN. *Modern Electrochemistry: An Introduction to an Interdisciplinary Area*. Plenum Press; 1977. <https://books.google.it/books?id=5nYyHQAACAAJ>.
5. Greiner W, Rischke D, Neise L, Stöcker H. *Thermodynamics and Statistical Mechanics*. Springer New York; 2012. <https://books.google.com.au/books?id=8jrTBwAAQBAJ>.
6. Ullmann F, Bohnet M. *Ullmann's Encyclopedia of Industrial Chemistry*. Wiley-VCH; 2003. <https://books.google.com.au/books?id=3Y1UAAAAMAAJ>.
7. Larminie J, Dicks A. *Fuel Cell Systems Explained.*; 2004. doi:10.1016/S0378-7753(00)00571-1
8. Santarelli M. Celle a combustibile a ossidi solidi (SOFC). *Modello elettrochimico*. (3):1-18.
9. Wang S, Jiang SP. Prospects of fuel cell technologies. *Natl Sci Rev.* 2017;4(2):161-163. doi:10.1093/nsr/nwx032
10. Ralph TR, Hogarth MP. Catalysis for Low Temperature Fuel Cells. *Reading*. 2002;46(January):117-135. doi:10.1595/147106707X180891
11. McLean G. An assessment of alkaline fuel cell technology. *Int J Hydrogen Energy*. 2002;27(5):507-526. doi:10.1016/S0360-3199(01)00181-1
12. Litster S, McLean G. PEM fuel cell electrodes. *J Power Sources*. 2004;130(1-2):61-76. doi:10.1016/j.jpowsour.2003.12.055
13. Jiang S. A comparison of O₂ reduction reactions on porous (La, Sr) MnO₃ and (La, Sr)(Co, Fe) O₃ electrodes. *Solid State Ionics*. 2002;146:1-22. doi:http://dx.doi.org/10.1016/S0167-2738(01)00997-3
14. Ai N, Jiang SP, Lü Z, Chen K, Su W. Nanostructured (Ba,Sr)(Co,Fe)O_{3-δ} Impregnated (La,Sr)MnO₃ Cathode for Intermediate-Temperature Solid Oxide Fuel Cells. *J Electrochem Soc.* 2010;157(7):B1033. doi:10.1149/1.3428366
15. Yoo S, Jun A, Ju YW, et al. Development of double-perovskite compounds as cathode materials for low-temperature solid oxide fuel cells. *Angew Chemie - Int Ed.* 2014;53(48):13064-13067. doi:10.1002/anie.201407006
16. Zhang Y, Knibbe R, Sunarso J, et al. Recent Progress on Advanced Materials for Solid-Oxide Fuel Cells Operating Below 500 °C. *Adv Mater.* 2017;29(48). doi:10.1002/adma.201700132
17. Angeltveit M. Development of Composite Cathodes for Solid Oxide Fuel Cells. 2017.
18. Agun L, Abd. Rahman H, Ahmad S, Muchtar A. Durability and Stability of LSCF Composite Cathode for Intermediate-Low Temperature of Solid Oxide Fuel Cell (IT-LT SOFC): Short Review. *Adv Mater Res.* 2014;893(July 2014):732-737. doi:10.4028/www.scientific.net/AMR.893.732
19. Berenov A, Atkinson A, Wood H. Evaluation of La_{0.8}Sr_{0.2}Cu_{1-x}Mn_xO_d Double

- Perovskite for Use in SOFCs. *ECS Trans.* 2007;7(1):1173-1181.
20. Perry Murray E, Sever MJ, Barnett SA. Electrochemical performance of (La,Sr)(Co,Fe)O₃-(Ce,Gd)O₃ composite cathodes. *Solid State Ionics.* 2002;148(1-2):27-34. doi:10.1016/S0167-2738(02)00102-9
 21. Petric A, Huang P, Tietz F. Evaluation of La-Sr-Co-Fe-O perovskites for solid oxide fuel cells and gas separation membranes. *Solid State Ionics.* 2000;135(1-4):719-725. doi:10.1016/S0167-2738(00)00394-5
 22. Bucher E, Egger A, Ried P, Sitte W, Holtappels P. Oxygen nonstoichiometry and exchange kinetics of Ba_{0.5}Sr_{0.5}Co_{0.8}Fe_{0.2}O_{3-δ}. *Solid State Ionics.* 2008;179(21-26):1032-1035. doi:10.1016/j.ssi.2008.01.089
 23. Wei B, Lü Z, Huang X, et al. Crystal structure, thermal expansion and electrical conductivity of perovskite oxides Ba_xSr_{1-x}Co_{0.8}Fe_{0.2}O_{3-δ} (0.3 ≤ x ≤ 0.7). *J Eur Ceram Soc.* 2006;26(13):2827-2832. doi:10.1016/j.jeurceramsoc.2005.06.047
 24. Skinner SJ, Kilner JA. Oxygen ion conductors. *Mater Today.* 2003;6(3):30-37. doi:10.1016/S1369-7021(03)00332-8
 25. Hayashi H. Thermal expansion of Gd-doped ceria and reduced ceria. *Solid State Ionics.* 2000;132(3-4):227-233. doi:10.1016/S0167-2738(00)00646-9
 26. Chen K, Liu S-S, Ai N, Koyama M, Jiang SP. Why solid oxide cells can be reversibly operated in solid oxide electrolysis cell and fuel cell modes? *Phys Chem Chem Phys.* 2015;17(46):31308-31315. doi:10.1039/C5CP05065K
 27. Chen K, Li N, Ai N, et al. Direct application of cobaltite-based perovskite cathodes on yttria-stabilized zirconia electrolyte for intermediate temperature solid oxide fuel cells. *J Mater Chem A.* 2016;00:1-7. doi:10.1039/C6TA07067A
 28. Baharuddin NA, Rahman HA, Muchtar A, Sulong AB, Abdullah H. Development of lanthanum strontium cobalt ferrite composite cathodes for intermediate- to low-temperature solid oxide fuel cells. *J Zhejiang Univ Sci A.* 2013;14(1):11-24. doi:10.1631/jzus.A1200134
 29. Li M, Hua B, Luo JL, et al. Enhancing Sulfur Tolerance of Ni-Based Cermet Anodes of Solid Oxide Fuel Cells by Ytterbium-Doped Barium Cerate Infiltration. *ACS Appl Mater Interfaces.* 2016;8(16):10293-10301. doi:10.1021/acsami.6b00925
 30. Juhl M, Primdahl S, Manon C, Mogensen M. Performance/structure correlation for composite SOFC cathodes. *J Power Sources.* 1996;61(1-2):173-181. doi:10.1016/S0378-7753(96)02361-0
 31. Preux N, Rolle A, Vannier RN, Nationale E. Electrolytes and ion conductors for solid oxide fuel cells (SOFCs). 2012:370-401.
 32. Electrochemistry P, Elements C, Equivalent C, Models C. Basics of Electrochemical Impedance Spectroscopy. *Princet Appl Res.* 2006;Applicatio(215):1-31. doi:10.1152/ajpregu.00432.2003
 33. He S, Chen K, Saunders M, Li J, Cui CQ, Jiang SP. A FIB-STEM Study of La_{0.8}Sr_{0.2}MnO₃ Cathode and Y₂O₃-ZrO₂/Gd₂O₃-CeO₂ Electrolyte Interfaces of Solid Oxide Fuel Cells. *J Electrochem Soc.* 2017;164(13):F1437-F1447. doi:10.1149/2.1061713jes
 34. Chen J, Liang F, Liu L, et al. Nano-structured (La, Sr)(Co, Fe)O₃+ YSZ composite cathodes for intermediate temperature solid oxide fuel cells. *J Power Sources.* 2008;183(2):586-589. doi:10.1016/j.jpowsour.2008.05.082
 35. Park YM, Kim JH, Kim H. High-Performance composite cathodes for solid oxide fuel cells. *Int J Hydrogen Energy.* 2011;36(15):9169-9179. doi:10.1016/j.ijhydene.2011.04.075
 36. Li N, Ai N, He S, et al. Effect of Pd doping on the activity and stability of directly

- assembled $\text{La}_{0.95}\text{Co}_{0.19}\text{Fe}_{0.76}\text{Pd}_{0.05}\text{O}_{3-\delta}$ cathodes of solid oxide fuel cells. *Solid State Ionics*. 2018;316(December 2017):38-46. doi:10.1016/j.ssi.2017.12.020
37. Magnone E. A Systematic Literature Review on BSCF-Based Cathodes for Solid Oxide Fuel Cell Applications. *J Fuel Cell Sci Technol*. 2010;7(6):64001. doi:10.1115/1.4001323
38. Chen K, Li N, Ai N, Cheng Y, Rickard WDA, Jiang SP. Polarization-Induced Interface and Sr Segregation of *in Situ* Assembled $\text{La}_{0.6}\text{Sr}_{0.4}\text{Co}_{0.2}\text{Fe}_{0.8}\text{O}_{3-\delta}$ Electrodes on $\text{Y}_2\text{O}_3\text{-ZrO}_2$ Electrolyte of Solid Oxide. *ACS Appl Mater Interfaces*. 2016;8(46):31729-31737. doi:10.1021/acsami.6b11665
39. Ai N, He S, Li N, et al. Suppressed Sr segregation and performance of directly assembled $\text{La}_{0.6}\text{Sr}_{0.4}\text{Co}_{0.2}\text{Fe}_{0.8}\text{O}_{3-\delta}$ oxygen electrode on $\text{Y}_2\text{O}_3\text{-ZrO}_2$ electrolyte of solid oxide electrolysis cells. *J Power Sources*. 2018;384(February):125-135. doi:10.1016/j.jpowsour.2018.02.082

9 Ringraziamenti

Alla mia famiglia e soprattutto ai miei genitori, che hanno sempre saputo sostenermi in ogni mia scelta.

Ad Alice, che ogni giorno mi fa innamorare come se fosse la prima volta, e alla sua famiglia, che mi ha accolto a braccia aperte.

Al professor Santarelli e al professor Jiang, che mi hanno permesso di vivere un'esperienza straordinaria.

Alla professoressa Carello, al Team H₂politO e a tutti i suoi componenti, con i quali ho condiviso emozioni uniche ed indimenticabili.

A Lorenzo, a Shuai e a tutti i membri del gruppo di ricerca del Building 614, che mi hanno accompagnato nel raggiungimento di quest'ultimo traguardo.

A Carolina, che fin dall'inizio di questa lunga avventura è sempre stata pronta a darmi una mano.

A Luca, Riccardo, Cesare e Camilla, che mi hanno accolto in casa loro diventando una seconda famiglia.

Al gruppo dei "Cinghiali", che tra una risata e l'altra, mi ha reso questo percorso molto più leggero.

Agli amici di sempre, Gianmarco e Lorenzo, che nonostante la distanza ci sono e ci saranno comunque.

A tutti voi, semplicemente, grazie.